Age and geochemistry of tephra layers from Ischia, Italy: constraints from proximal-distal correlations with Lago Grande di Monticchio

Emma L. Tomlinson[1*], Paul G. Albert[1,^], Sabine Wulf[2], Richard J. Brown[3], Victoria C. Smith[4], Jörg Keller[5], Giovanni Orsi[7], Anna J. Bourne[8^], Martin A. Menzies[1]

[1]Department of Earth Sciences, Royal Holloway University of London, Egham, UK

[2]GFZ German Research Centre for Geosciences, Section 5.2 – Climate Dynamics and Landscape Evolution, Potsdam, Germany

[3]Department of Earth Sciences, Science Labs, Durham University, Durham, UK

[4]Research Laboratory for Archaeology and the History of Art, University of Oxford, Oxford, UK

[5]Institute of Geosciences, Mineralogy and Geochemistry, Albert-Ludwigs-University Freiburg, Freiburg, Germany

[7]Instituto Nazionale di Geofisica e Vulcanologia, Sezione di Napoli-Osservatorio Vesuviano, Napoli, Italy.

[8]Centre of Quaternary Research, Department of Geography, Royal Holloway University of London, Egham, UK

*Present address: Department of Geology, Trinity College Dublin, Dublin, Ireland

^Present address: Department of Geography, College of Science, Swansea University, Swansea, UK.

Corresponding author: tomlinse@tcd.ie

Abstract

Unraveling the eruptive history of the Island of Ischia (southern Italy) is problematic due its to burial, caldera collapse, resurgent uplift and erosion. Here, we present new major and trace element glass data for 39-75 ka proximal tephra deposits, including the caldera-forming Monte Epomeo Green Tuff (MEGT) eruption. Correlations with the distal tephra archive preserved at Lago Grande di Monticchio (LGdM) are used to constrain the timing of yet undated eruptive events. Out of 13 LGdM tephras analysed from the 39-104 ka time window, glass geochemical data show all are compositionally consistent with explosive

volcanism erupted on Ischia, whilst 5 of these could be correlated with specific proximal deposits..

Pre-MEGT pyroclastic sequences comprise three compositional groups, these groups occur repeatedly in sucessive eruptions. Proximal-distal correlations indicate that the Porticello and Tisichiello eruptions occurred at 76 ± 3 ka and 59 ± 2 ka, respectively. The MEGT eruption is correlated with LGdM TM-19, which has been directly dated at 55 ± 2 ka. Post-MEGT tephras form compositional groups that overlap with the pre-MEGT but are displaced to lower FeO and TiO_2 and lower incompatible element contents. Proximal-distal correlations indicate that the Schiappone and Pietre Rosse eruptions occurred at 50.6 ± 2.0 ka and 45 ± 6 ka, respectively.

Tephra from the MEGT eruption span a wide compositional range, broadly overlapping the three pre-MEGT compositional groups but are displaced to higher Nd and Y and contain an additional less evolved glass population. Glass geochemistry is used to recognise and confirm distal equivalents of the MEGT at LGdM (TM-19) and in the Ionian (Y-7), Adriatic (PRAD 1870) and Tyrrhenian (C-18, MD 28) seas. Distal occurences of MEGT tephra define a dispersal axis to the south-southeast and are found as far as 540 km from Ischia, making MEGT one of the most widely dispersed late Quaternary pyroclastic deposit erupted in the Campanian region. We have estimated a volume of approximately 40 km^3 for the fallout portion of the MEGT pyroclastic sequence on the basis of proximal and distal deposit thicknesses.

Keywords: tephrochronology; volcanic ash; Ischia; explosive eruptions; quaternary volcanism; Campanian volcanic field

1. Introduction

Knowledge of past eruptive behaviour is critical for volcanic hazard assessment and for defining future eruption scenarios. Distal tephra archives can provide valuable information about eruptive histories, as well as information about the long-term chemical evolution of a volcanic-magmatic system. This is particularly useful in cases where unravelling eruptive history from proximal deposits is problematic, for example where outcrop is limited by poor exposure or where the stratigraphic record is incomplete due to erosion or deposition at sea, such as is common at island volcanoes (e.g., Brown and Branney 2013; Cassidy et al., 2014).

The volcanic island of Ischia, southern Italy, has been characterised by alternating periods of intense volcanic activity, resurgence, and quiescence (Orsi et al. 1991; 1996; de Vita et al., 2006) since ca.150 ka (Poli et al., 1987; Gillot et al. 1982; Vezzoli 1988). The largest eruption was the 56 ka (Gillot et al., 1982) caldera-forming Monte Epomeo Green Tuff (MEGT). Much of the present knowledge about Ischia's volcanic past has come from study of proximal deposits, which are incomplete, poorly exposed and heavily eroded (e.g., Brown et al., 2008). Located one hundred and fifty kilometres to the east of Ischia, the annually laminated (varved) sediments of Lago Grande di Monticchio (LGdM; Fig. 1) span 3-133 ka and provide a key tephra archive of volcanism in the region (Wulf et al., 2004). LGdM is ideally positioned along the dominant downwind dispersal axes of volcanic plumes from the Phlegraean Volcanic District and numerous tephra layers in the LGdM record have been attributed to Ischia (Wulf et al., 2008; 2012). From a hazard assessment perspective, this same dispersal axis passes over the now heavily populated city of Naples. The LGdM sedimentary record provides a precise stratigraphy and independent (varve) chronology, which is essential for constraining the eruptive history of Ischia. Explosive activity at Ischia has produced several important widespread tephra markers that were dispersed widely across the Tyrrhenian, Ionian and Adriatic seas (e.g. Keller et al., 1978; Paterne et al., 1988; Tamburino, 2008; Bourne et al., 2010). These include the Y-7 tephra from the Ionian

Sea (Keller et al., 1978) and the C-18, C-17 and C-16 layers from the Tyrrhenian Sea (Paterne et al., 1986, 1988). The C-17 tephra has been correlated with the MEGT eruption (Paterne et al., 1986, 1988), while Y-7 was previously linked to an older Ischia eruption, the Sant'Angelo Tephra (Keller et al., 1978; Wulf et al., 2004). However, Paterne et al. (1988) linked the C-18 layer to the Y-7 layer, and this highlights some of the uncertainty as to the correlations and age of these marker tephra.

In this contribution, we provide micron-beam major and trace element data for Ischia glasses from proximal tephra outcrops, this data is essential for precisely assigning distal tephra to explosive activity at Ischia. Furthermore, we also present multi-elemental glass data from suspected Ischia distal tephra layers recorded within the LGdM tephra record, and other key distal localities in the Ionian and Adriatic Seas. The distal tephra layers investigated here span 104-39 ka and record volcanic eruptions that are likely to be found in other sedimentary archives across the Mediterranean. We define diagnostic geochemical fingerprints for key Ischia tephra layers and provide proximal-distal correlations for a number of important eruptions. The correlations defined herein are used to: 1) constrain the ages eruptions at Ischia; 2) assess the temporal variation in the composition of Ischia products; and 3) evaluate the dispersal axis of the MEGT and calculate the volume of the fall component.

2. Background

The volcanic island of Ischia, located in the Tyrrhenian Sea, at the northwestern corner of the Bay of Naples, is the most westerly volcano in the Phlegraean Volcanic District, which also includes Campi Flegrei and Procida–Vivara. Ischia is a caldera with a complex volcanic and structural history. The oldest dated rocks on the Island are a series of lava flows, tuffs and scoria cones erupted at 150 ka (Poli et al., 1987; Gillot et al. 1982; Vezzoli 1988), however magnetic data indicate that Ischia is the remnant of an older, larger volcanic

complex extending to the west of the island (Orsi et al. 1999; Bruno et al. 2002). The 7 x 10 km caldera was formed during the 56 ka MEGT eruption (Gillot et al., 1982). The centre of the caldera has been uplifted by resurgence to a height of 789 m above sea level over the past 30 ka, forming the Monte Epomeo resurgent block. The most recent eruption was in 1302 AD and on-going earthquakes, thermal springs and fumarolic activity (Buchner et al., 1996; Di Napoli et al., 2009, 2011 and references therein) indicate that Ischia is still active. Erupted magmas are dominantly alkali-trachytes, with subordinate shoshonite, latite and phonolite (Poli et al., 1987; Crisci et al., 1989; Civetta et al., 1991; Piochi et al., 1999).

Volcanic activity at Ischia is characterised by alternating periods of resurgence, intense volcanic activity and quiescence (Orsi et al. 1991; 1996; de Vita et al., 2006; Vezzoli et al., 2009), with Post-MEGT activity occurring in three cycles (55 – 33 ka; 28 – 18 ka; 10 ka – 1302 AD; Civetta et al., 1991). The period of interest for this study spans 75-39 ka, starting at the time at which explosive activity began at Ischia, at ~ 75 ka BP. We include the caldera-forming MEGT eruption and the oldest succeeding explosive eruptions of the first cycle (55 – 33 ka) identified by Civetta et al. (1991).

The 75-60 ka period was dominated by intense explosive volcanic activity characterized by numerous magmatic and phreatomagmatic eruptions (Brown et al., 2008; Sbrana et al., 2009). The eruptions were fed by phono-trachytic magmas and their deposits, include the Sant'Angelo Tephra, Olummo, Tisichiello and Porticello units of Brown et al. (2008).

The 55-33 ka cycle of activity of Civetta et al. (1991) began with the caldera-forming eruption of the Monte Epomeo Green Tuff (MEGT) (Vezzoli 1988; Tibaldi and Vezzoli 1998; Brown et al., 2008). The MEGT was fed by the compositionally most variable of the Ischia magmas. Post-MEGT activity, extruded trachytic to latitic magmas, and comprised magmatic and phreatomagmatic eruptions that generated the fallout and pyroclastic density

current (PDC) deposits. These include the Schiappone unit of Brown et al. (2008), and the Pietre Rosse, and Agnone units of Civetta et al. (1991).

3. Samples

3.1 Proximal samples

Herein, we have focused on the eruptions that are likely to have led to the widespread dispersal of tephra. The investigated eruptions are those that have produced (from oldest to youngest) the Pre-MEGT Sant'Angelo Tephra, Olummo Tephra, Tisichiello Tephra, Porticello tephra, and MEGT (Brown et al., 2008), and Post-MEGT Schiappone Tephra (Brown et al., 2008), Pietre Rosse Tuff and Agnone Tuff (Civetta et al., 1991). The sampled localities are shown in figure 1b.

The Sant'Angelo Tephra sequence (termed the Unità di Monte Sant'Angelo (UMSA) by Rosi et al. 1988) is a series of decimetre thick pumice fall deposits and ignimbrites overlain by block and ash flow deposits (Brown et al., 2008). The Sant'Angelo Tephra is limited to one outcrop in the south of Ischia, leading Brown et al. (2008) to suggest that they formed as a result of small-volume explosive and effusive eruptions. It has been interpreted as a precursor to, or the first distinct phase of, the MEGT cycle (Rosi et al., 1988; Vezzoli, 1988; Morche 1988; Wulf et al. 2004; Kraml 1997). The position of the Sant'Angelo Tephra relative the Olummo, Tisichiello and Porticello tephras is not known as they are not found together in stratigraphic section (Brown et al., 2008; Table 1).

The Olummo, Tisichiello and Porticello tephras are a succession of 3.5 to >7 m thick bedded pumice and ash fall deposits separated by paleosols (Brown et al., 2008), these are classified as the deposits of sub-Plinian eruptions (Brown et al., 2014). A block-and-ash flow deposit caps the Olummo Tephra (Brown et al., 2008). The Olummo, Tisichiello and Porticello tephras form part of the Pignatiello Formation of Forcella et al. (1982) and Vezzoli

(1988) and overly the scoria breccia of the 74 ka Parata formation (Vezzoli et al., 1988).

MEGT pumice fall deposits exceed 8 m thick are exposed in extracaldera locations along the southern coast of Ischia. They are overlain by ignimbrites and lithic breccias that can be traced to Procida and western Campi Flegrei (Brown et al., 2008). The lower ignimbrite is ~70 m thick, while the upper ignimbrite reaches 200 m thick. They are separated by vitric siltstone and sandstone that indicate a hiatus during the eruption (Brown et al., 2008). K-Ar age determinations for the intracaldera ignimbrite range from to 51 ka to 59 ka, excluding those with large errors (Gillot et al., 1982).

The Schiappone tephra comprises a 7 m pumice fall deposit intercalated with ignimbrites and is likely to represent Plinian activity (Brown et al., 2014). This is overlain by a >60 m thick massive ignimbrite (Brown et al., 2008). The Schiappone tephra was previously interpreted as extracaldera deposits of the MEGT (Rosi et al. 1988; Vezzoli 1988).). K-Ar age determinations for the Schiappone tephra range from 48-52 ka (Vezzoli 1988, for units previously correlated with the MEGT).

The Pietre Rosse and Agnone tuff units are exposed in the southwest and northwest corners of Ischia and comprise bedded pumiceous tuffs with interbedded cross-stratified ignimbrites (Civetta et al., 1991). K-Ar dating indicates ages of 44-48 ka and 39-45 ka for the Pietre Rosse and Agnone tuffs, respectively (Poli et al., 1987). These deposits were collectively termed the Citara-Serrara Fontana Formation by Rittmann (1930).

The characteristics of all samples investigated, including colour and mineral assemblages, are summarised in table 1. Samples below and including Schiappone are described and stratigraphic columns are presented in Brown et al. (2008; 2014), whilst Pietre Rosse and Agnone tuff samples follow Brown et al. (2008; 2014) and Civetta et al. (1991).

193

194 **3.2 Distal samples**

195 *3.2.1 Lago Grande di Monticchio (LGdM)*

196 The laminated sediments at LGdM (Fig.1a) provide a high-precision varve age and
197 sedimentation rate record (Brauer et al., 2007) with an incremental counting error on LGdM
198 varve ages of 5-10 % (Wulf et al., 2012). We have determined the major and trace element
199 concentrations of 13 tephra layers in the LGdM core, that are thought to have originated
200 from Ischia between 39 and 104 ka BP (Table 2). We focus on tephra layers that are > 1mm
201 thick, these layers include TM-19 and TM-20, that were previously correlated to the MEGT
202 and Sant'Angelo Tephra, respectively (Wulf et al., 2004).

203

204 *3.2.2 Stromboli Island (Aeolian Islands)*

205 Exotic volcanic deposits on the Aeolian Islands provide a useful record of major ash
206 dispersals sourced from the Italian mainland and, in particular, from the Campanian region
207 (Keller 1981; Morche 1988). The '*Ischia tephra*' layer was first recognised on the Island of
208 Salina (Keller 1969), but also outcrops on Filicudi, Lipari, Panarea and Stromboli (Keller
209 1969, 1980; Morche 1988; Lucchi et al., 2008). On the island of Stromboli the tephra layer
210 occurs on the eastern lower flank of the volcano and is referred to as the '*Ischia tephra*
211 *Stromboli'* (ITS) (Morche 1988; Hornig-Kjarsgaard et al. 1993; Kraml 1997). Following
212 Morche (1988) and Hornig-Kjarsgaard et al. (1993), this yellow ash layer on Stromboli is up
213 to 25-30 cm thick and is inter-bedded within locally derived scoriaceous lapilli deposits. The
214 tephra of our sample ITS contained K-feldspar, biotite, plagioclase, clinopyroxene and the
215 key index minerals titanite (sphene, $CaTiSiO_5$) and yellow acmite in order of decreasing
216 abundance. The ITS tephra on Stromboli has been directly dated by $^{40}Ar/^{39}Ar$ analyses of
217 sanidine grains to 56 ± 4 ka (Kraml, 1997).

218

219 *3.2.3 M25/4-11 (Ionian Sea)*

Four piston cores (M25/4-10 to 13) were retrieved in 1993 from the Calabrian Rise (36.7542 N; 17.1806 E) in the Ionian Sea as part of a specific tephrochronology project during cruise M25 of R/V *Meteor* (Keller 1994). All four cores contained the Y-7 tephra layer in the Y-zone in stratigraphic sequence. The studied Y-7 tephra was retrieved in piston core M25/4-11 (36.7542 N; 17.1806 E). The Y-7 tephra occurs at a depth of 223-225 cm, above but close to the MIS 3/4 transition (Keller 1978; Negri et al. 1999; Kraml, 1997). The Y-7 tephra layer contains K-feldspar, biotite, plagioclase, clinopyroxene, titanite and acmite, in a decreasing order of abundance. The astronomically calibrated sapropel chronology and the oxygen isotope chronology give interpolated ages of ca. 50 ka for the Y-7 tephra (Kraml 1997; Negri et al. 1999).

3.2.4 PRAD 1-2 (Adriatic Sea)

PRAD 1-2 was recovered from the western and upper flank of the Mid-Adriatic deep (42.6763 N; 14.7704 E) at 185.5 m water depth (Bourne et al., 2010). The cryptotephra layer PRAD-1870 was identified at 1870 cm depth and stratigraphically lies above the MIS 3/4 transition. The glass shards are typically platy and colourless (Bourne et al. 2010).

4. Analytical Methods

Proximal pumice clasts were crushed and clean fragments from the interiors of up to thirty individual clasts were picked and mounted in ‘Stuers EpoFix’ epoxy resin for analysis. Individual shards of distal tephra were also mounted in Stuers EpoFix for geochemical micro-beam analysis.

4.1 Electron Micro-Probe Analysis (EMPA)

Major element concentrations of individual glass shards of proximal and distal tephra samples were determined using JEOL JXA-8600 electron microprobe, equipped with 4 spectrometers and SamX software, at the Research Laboratory for Archaeology and the

History of Art, University of Oxford. An accelerating voltage of 15 kV, low beam current (6 nA), and defocused (10 μm) beam were used to minimize Na migration. Count times were 30 s on each peak, except for Na (10 s) and P and Cl (60 s). The instrument was calibrated for each set of beam conditions using a suite of appropriate mineral standards. The calibration was verified using a range of secondary glass standards from the Max Planck Institute. Count rates were corrected using the PAP absorption correction method. Sample totals are normalised to 100 wt% in all plots and tables. Analytical precision is <10% relative standard deviation (%RSD) for analyses with concentrations >0.8 wt%. Error bars on plots represent the 2x standard deviation of replicate analyses of MPI-DING StHs6/80-G.

4.2 Laser Ablation Inductively Coupled Plasma Mass Spectrometry (LA-ICP-MS)

LA-ICP-MS analyses of glass shards of proximal and distal tephra were performed using an Agilent 7500es coupled to a Resonetics 193 nm ArF excimer laser-ablation system (RESOlution M-50 prototype) with a two-volume ablation cell (Muller et al., 2009) at the Department of Earth Sciences, Royal Holloway University of London. We used 34, 25 and 20 μm laser spots, depending on the size of the area available for analysis in different samples. The repetition rate was 5 Hz and the count time was 40 s (200 pulses) on the sample and 40 s on the gas blank (background). Concentrations were calibrated using NIST612 with ^{29}Si as the internal standard. Data reduction was performed manually using Microsoft Excel allowing removal of portions of the signal compromised by the occurrence of microcrysts. Full details of the analytical and data reduction methods are given in Tomlinson et al. (2010). Accuracies of ATHO-G and StHs6/80-G MPI-DING glass analyses are typically <5% for most elements and <10% for Nb, Pr, Eu, Gd, and Ta. Reproducibility of StHs6/80-G analyses is <5 RSD% for all trace elements. For consistency with EMPA error reporting, error bars on plots represent the 2 standards deviation of replicate analyses of StHs6/80-G. Relative standard errors (RSE) for LA-ICP-MS tephra samples analyses are typically <2 % for Rb, Sr, Zr, Nb, Ce, Pr; <5% for V, Y, Ba, La, Nd, Sm, Th, U, and <10% for

Eu, Dy, Er, Yb, Lu.

4.3 Assessment of tephra correlations

Proximal-distal glass correlations are assessed on the basis of (1) visual assessment using a range of major and trace element biplots; (2) multi-element plots in which each tephra is normalised to its proposed proximal equivalent; and (3) statistical distance (D^2) tests. The statistical distance is a measure of the difference between pairs of samples based on both mean and standard deviation (see Perkins et al., 1995). Providing sample pairs are normally distributed, the $D^2_{calculated}$ value will have a Chi-squared distribution between compositionally identical sample pairs. Where the $D^2_{calculated}$ value is greater than the $D_{2critical}$ value then the null hypothesis (that the sample pairs are identical) must be rejected. A $D^2_{calculated}$ value less than the $D^2_{critical}$ means that the sample pairs cannot be distinguished, however, this does not confirm they are identical. Compositionally identical samples can only be determined if the $D^2 = 0$. In some cases significant statistical distance between tephra units cannot be shown. However, lower D^2 values relative to other sample pairs may indicate greater compositional similarity (Pearce et al., 2008) and provide further confidence in possible correlations as determined by alternative and previously mentioned comparison approaches. Confidence limits (*p*) values for statistical distance values are defined from the Chi-squared table and depends on the degrees freedom (*f*). *f* = the number of elements used to generate the D^2 values. For major elements we used all elements excluding MnO, P_2O_5 and Cl (thus *f* = 8) and for trace element *f* = 11 (Rb, Y, Zr, Nb, La, Ce, Pr, Nd, Sm, Th U). At the 95% confidence limit the $D^2_{critical}$ values for majors and trace elements are 15.5 and 19.7 respectively.

5. Results

Representative major and trace element analyses of proximal glasses are reported in table 3 and the full dataset is available as supplementary data. In presenting the results we will

highlight the compositional features that allow the discrimination of different eruptive units thus revealing the diagnostic chemistry that can be used as a fingerprints in proximal-distal tephra correlations.

5.1 Proximal glass chemistry

Volcanic glasses produced during explosive eruptions from Ischia are dominantly intermediate silicic (60.6-63.0 wt%) and straddle the phonolite-trachyte boundary (Fig. 2a), a characteristic shared by magmas from the other active Neapolitan volcanoes (Campi Flegrei and Somma-Vesuvius). Proximal Ischia phonolite and trachyte glasses have restricted compositional ranges and show an overall trend of increasing CaO and K_2O and decreasing FeO, Na_2O (Fig. 2b) and total alkalis with increasing SiO_2. They can be distinguished from other Neapolitan magmas by their lower CaO concentrations (<1.80 wt%) (Fig. 2c,d). Proximal Ischia trachyte and phonolite glasses are alkali-rich, with high total alkalis (Na_2O+K_2O = 12.8-14.7 wt%) and high K_2O (>5.8 wt%), therefore Ischia tephras often have K_2O/Na_2O <1 (e.g. Poli et al., 1987) reaching as low as K_2O/Na_2O = 0.7. Mantle-normalised trace element concentrations of proximal Ischia glasses have subduction-related signatures with depletion in the HFSE element relative to the LILE and pronounced depletion in Ba, Sr and Eu in response to the fractionation of K-feldspar, a dominant phenocryst phase in juvenile clasts. Proximal Ischia glasses are highly evolved (Zr/Sr=0.2-600, mean = 128), extending to more highly evolved compositions than Campi Flegrei and Vesuvius tephra), and span a narrow range of Nb/Th (2.3 ± 0.3), partially overlapping with the pre-CI trend (Tomlinson et al., 2012).

5.1.1 Pre-MEGT (4 eruptions)

Pre-MEGT glasses are phonolitic to phono-trachytic (Fig. 2a). Using decreasing CaO as a fractionation index reveals a decrease in K_2O and an increase in Na_2O as evolution progresses (Fig. 3a-c). This gives rise to a wide range of alkali compositions in the pre-

MEGT tephra (K_2O/Na_2O 0.7 to 1.1). Trace element contents increase sharply with decreasing CaO with Th going from 20 to 80 ppm and Zr from ~300 to ~1100 ppm (Fig. 4a-c). Major and trace element compositional clusters within both the proximal and distal tephra allow two compositional groups to be defined within the pre-MEGT magmatic system

Pre-MEGT Group 1 glasses have higher incompatible element/Th ratios (Y/Th = 1.5 ± 0.5; Ta/Th = 0.12 ± 0.04 and Nd/Th 2.4 ± 0.8). On the basis of a compositional gap at Th = 30−36 ppm and Zr = 432−550 ppm, they are divided in two sub-groups. Group 1a, with Th<30 ppm, includes the least evolved glasses with high CaO (1.36 ± 0.05 wt%), SiO_2 (62.3 ± 0.2 wt%) and K_2O (7.0 ± 0.1 wt%), low FeO (2.5 ± 0.1 wt%) and Na_2O (6.8 ± 0.2 wt%; giving K_2O/Na_2O = 0.97−1.11) and low incompatible trace element concentrations (Zr < 440 ppm, Nb <57 ppm). Group 1b, with Th>36 ppm, is composed of intermediate glasses with low CaO (1.14 ± 0.08 wt%), intermediate SiO_2 (61.9 ± 0.2 wt%), FeO (2.6 ± 0.1 wt%), K_2O (6.5 ± 0.2 wt%) and Na_2O (7.4 ± 0.2 wt%; giving K_2O/Na_2O 0.72−0.95) and moderate incompatible trace element concentrations (Zr = 550−695 ppm, Nb = 95−115 ppm).

Pre-MEGT Group 2 glasses have lower incompatible element/Th ratios (Y/Th = 1.2 ± 0.2; Ta/Th = 0.10 ± 0.01 and Nd/Th 1.8 ± 0.2) forming sub-parallel trend on incompatible element bivariate plots. They are the most evolved among the Pre-MEGT rocks, with low CaO (1.05 ± 0.06 wt%) and K_2O (6.1 ± 0.1 wt%), and high FeO (2.8 ± 0.2 wt%), Na_2O (8.2 ± 0.2 wt%) and SiO_2 (61.3 ± 0.4 wt%), giving K_2O/Na_2O 0.68−0.78. Incompatible trace element contents are high (Th ≥ 40 ppm, Zr > 610 ppm, Nb > 80 ppm).

These compositional groups occur repeatedly in successive Pre-MEGT eruptions as shown in Table 4. Tephra from potentially smaller-volume eruptions (e.g. Sant'Angelo and Porticello tephras) are composed of glasses from only one of the magma groups, while those from apparently larger-volume eruptions (e.g. the Tisichiello and Olummo tephras)

355 display glasses from all three compositional groups. The repeated occurrence of these
356 magma groups is problematic for proximal-distal and distal-distal tephra correlations.
357 However, small differences in major and trace element absolute abundances between
358 successive deposits of a given compositional group may be used to fingerprint individual
359 eruptions.
360
361 ***5.1.2 MEGT***
362 Glasses in the extracaldera MEGT pumice fall deposit and overlying welded ignimbrite
363 straddle the phono-trachytic boundary and overlap with the least evolved glass
364 compositions of Pre-MEGT group 2. The MEGT glasses extend to less evolved
365 compositions than seen in the Pre-MEGT group 2, with CaO (0.88−1.05 wt%), FeO (2.3−2.7
366 wt%) and Na_2O (7.8−8.2 wt%) and higher K_2O (5.8−6.6 wt%) giving K_2O/Na_2O 0.7−1.4 (Fig.
367 3d-f). Incompatible trace element concentrations span a relatively narrow range (Th 49−58
368 ppm, Zr 679−846 ppm) and lack the more most elevated compositions seen in Pre-MEGT
369 group 2 glasses (Fig. 4d-f).
370
371 Pumice fragments from the lithic breccia at the top of the sequence form a trachytic cluster,
372 that lies beyond the less-evolved end of the Pre-MEGT Sub-group 1a glasses. Relative to
373 Pre-MEGT Sub-group 1a, the MEGT lithic breccia has higher FeO (2.7 ± 0.3 wt%), MgO
374 (0.51 ± 0.11 wt%) and K_2O (7.44 ± 0.5 wt%), higher but overlapping CaO (>1.34 wt%) and
375 lower Na_2O (6.1 ± 0.6 wt%) at constant SiO_2 (62.6 ± 0.4 wt%). The incompatible trace
376 element concentrations are the lowest detected in Ischia glasses at Th <16 ppm; Zr <242
377 ppm, Nb <46 ppm.
378
379 The green and grey pumices of the extracaldera MEGT ignimbrite at Acquamorta (Monte di
380 Procida) are phono-trachytic and overlap with Pre-MEGT group 1 (a and b), spanning a
381 range of CaO (1.04−1.29 wt%), Na_2O and K_2O (K_2O/Na_2O 0.8−1.0). Incompatible element

concentrations are variable (Th 24−56 ppm, Zr 367−834 ppm) and fall on a sub-parallel trend of higher Nb and Y for a given Th relative to the studied Pre- and Post-MEGT glasses.

5.1.3 Post-MEGT (3 eruptions)

Glasses from Post-MEGT deposits are dominantly trachytic and displaced to lower MgO, FeO and TiO_2 (down to 0.23, 2.1 and 0.42 wt%, respectively; Fig. 3g-l) and incompatible element (Th 13−74 ppm, Zr 211−841 ppm) contents relative to Pre-MEGT and MEGT glasses (Fig. 4g-l). Post-MEGT glasses show a general trend of decreasing CaO and K_2O, and increasing Na_2O, giving rise to a wide range of alkali compositions (K_2O/Na_2O 0.86−1.33), incompatible element concentrations increase with decreasing CaO. Major and trace element compositional clusters allow two compositional groups to be defined within the post-MEGT erupted rocks. Post-MEGT Group 1 glasses have higher incompatible element/Th ratios (Y/Th = 1.5 ± 0.2; Ta/Th = 0.13 ± 0.01 and Nd/Th 2.5± 0.4), similar, within error, to those of the Pre-MEGT Group 1. They span a wide compositional range from high to intermediate CaO (1.2−1.5 wt%), K_2O (6.6−7.7 wt%) and intermediate to low Na_2O (5.7 to 7.1 wt%), giving K_2O/Na_2O values between 0.94 and 1.33. Incompatible element contents are low to moderate (Zr = 210−556 ppm and Th = 13−43 ppm). Post-MEGT Group 2 glasses have lower incompatible element/Th ratios (Y/Th = 1.16 ± 0.05; Ta/Th = 0.10 ± 0.01 and Nd/Th = 1.7 ± 0.1), similar, within the errors, to those of the Pre-MEGT Group 2 glasses. They are the most evolved post-MEGT rocks, with low CaO (0.1−1.3 wt%), K_2O (6.4−6.6 wt%) and low Na_2O (7.0−75 wt%), giving K_2O/Na_2O 0.86-0.93, and moderate incompatible element contents (Zr 505-630 ppm and Th 35-47 ppm).

In the studied proximal Post-MEGT sequence, each compositional group is observed only in the deposits of one single eruption (Table 5), however, comparison of our glass data with whole rock data for the same tephra, at different field localities (Civetta et al., 1991), reveal that the Post-MEGT Pietre Rosse and Agnone Tuffs are bimodal in composition displaying

409 both compositional groups. This, coupled with fact that some post-MEGT Ischia tephra
410 layers detected in the distal LGdM record are bimodal, justifies our definition of
411 compositional groups for this period of the Ischia magmatic system. Whilst the Schiappone
412 Tephra and Agnone Tuff both belong to the same Post-MEGT compositional group, they
413 can be easily distinguished as the Agnone Tuff glasses are more enriched in their
414 incompatible trace element concentrations, whilst the Schiappone Tephra glasses have
415 higher K_2O/Na_2O ratios (Fig. 3). There is some overlap between Schiappone Tephra and
416 the MEGT lag Breccia, however, the Schiappone tephra glasses can be distinguished by
417 the absence of the higher MgO concentrations.
418
419 ***6. DISCUSSION***
420 In this section, we compare the data on proximal deposits presented above to new major
421 and trace element data for selected Ischia tephra layers from the distal LGdM archive
422 (Table 6), in order to better constrain the timing and frequency of eruptions at Ischia. Ages
423 presented for each LGdM tephra are given as calendar ages BP (1950) following the LGdM
424 varve and sedimentation rate chronology of Brauer et al. (2007). Where applicable, other
425 distally recognised tephra layers from other locations are also discussed. The distinctive
426 and prevalent MEGT tephra is used to divide the LGdM stratigraphy into Pre-MEGT and
427 Post-MEGT periods and so is discussed first.
428
429 **6.1 MEGT**
430 ***6.1.1 MEGT LGdM tephra correlations***
431 LGdM tephra TM-19 (60,060 varve years BP) is the thickest layer, and at a trace element
432 level is the most heterogeneous Ischia tephra layer recognised in the LGdM stratigraphic
433 sequence. The TM-19 layer comprises a 2 cm thick, coarse-grained ash fall layer overlain
434 by 30 cm of co-ignimbrite ash with minor sediment. Glass shards in the TM-19 layer are
435 heterogeneous and broadly overlap all three Pre-MEGT groups at a major, minor and trace

element level (Fig. 3-4). TM-19 tephras plotting in the Pre-MEGT Group 2 field match the proximal MEGT extra-caldera fall and overlying welded ignimbrite. Both the proximal MEGT fall and TM-19 tephra are restricted in terms of their overall levels of incompatible trace element enrichment and do not extend to the higher concentrations detected in the Pre-MEGT Group 2 rocks Sant'Angelo tephra (flow and lag breccia), Olummo Tephra (lower fall) and Tisichiello Tephra (upper fall). A second cluster of TM-19 glasses fall in the Pre-MEGT group 1 a and b field, but are displaced to higher concentrations of Nd, Sm, Ce and Y for a given Th (Fig. 5), relative to the Pre-MEGT Group 2 and match the extracaldera MEGT deposits from Acquamorta (Monte di Procida). TM-19 also has shards that match the composition of the least evolved MEGT glass population from the lithic breccia at the top of the extracaldera proximal sequence (Fig. 5). In summary the MEGT tephra investigated satisfies more of the compositional variation observed in heterogeneous TM-19 than any of the stratigraphically older or younger eruptive units, thus providing us with a strong correlation., This supports a distal-proximal correlation and re-affirms the interpretation of Wulf et al. (2004). Crucially, the stratigraphic integrity of the TM-19 tephra layer within the varved sediments of LGdM indicates that this compositional heterogeneity is diagnostic of the MEGT eruption.

6.1.2 Other distal MEGT equivalents

Other Mediterranean tephra layers that have been stratigraphically associated with early MIS 3 and attributed to explosive activity on Ischia have been re-investigated. These tephras include the southerly dispersed Ionian Sea Y-7 tephra (M25/4-11) and the 'Ischia tephra' layer on Stromboli (ITS) both of which were previously linked to the Sant'Angelo tephra (Keller et al., 1978; Kraml 1997; Lucchi et al., 2008). We have also investigated a marine cryptotephra PRAD 1870 from the Adriatic sea east of Ischia, which has been linked to MEGT (Bourne et al., 2010). Y-7, ITS and PRAD1870 show near identical trace element compositions and heterogeneity to TM-19 and to that of the proximal MEGT tephra

investigated (Fig. 5). Furthermore, glasses from the tephra MD 28 (southern Tyrrhenian Sea) appear to show similar heterogeneity consistent with the other distal MEGT equivalents (Fig. 5).

The earlier correlations of the southerly-dispersed Ionian Sea Y-7 (Keller et al., 1978; Kraml 1997) and ITS (Kraml 1997; Lucchi et al., 2008) to the Sant'Angelo Tephra are inconsistent with the glass data presented here. Only the most evolved components of these two distal tephra correspond to Sant'Angelo Tephra Pre-MEGT group 2 glass chemistries and this is equally satisfied by MEGT Plinian fall compositions. The Sant'Angelo Tephra does not match the full geochemical range observed in the Y-7, as it lacks the least evolved Pre-MEGT Group 1 compositions with $K_2O>Na_2O$ and also the intermediate glass compositions with higher Nd and Y for a given Th – both of which are found in the MEGT and present in the TM-19, Y-7 and ITS tephra layers (Fig. 5).

Other Tyrrhenian Sea ash layers deposited in early MIS 3 sediments showing high Na_2O (> 6.wt %) and low CaO content relative to other Campanian volcanic sources have been attributed to the explosive activity of Ischia (Paterne et al., 1986; 1988; Calanchi et al., 1994). The marine layer C-17, recognised by Paterne et al. (1986), was correlated to the caldera-forming MEGT eruption. The stratigraphically lower, thicker and more widespread C-18 tephra layer, was later tentatively correlated with the Ionian Sea Y-7 layer (Paterne et al., 1988; Calanchi et al., 1994), but remained proximally undefined on Ischia (Paterne et al., 1986; 1988; Calanchi et al., 1994). Whilst major data reveals Ischia as a proximal source, data are not directly comparable to proximal glasses presented herein owing to very different analytical parameters (i.e., SEM [Major elements] and neutron activation [Trace elements]. Bulk REE element analyses of glass separates are presented in Paterne et al. (1986). Remembering that bulk glass analyses homogenises any compositional variation, some observations can be made. The thicker, more widespread, C-18 shows significantly

higher levels of incompatible trace element enrichment (i,e,, Ce 222 ppm; Nd 73 ppm) relative to the C-17 tephra (i.e., Ce 157 ppm; Nd 48 ppm). C-18 concentrations appear to represent an average composition of the distal MEGT equivalents (TM-19, Y-7, ITS and PRAD 1870), whilst the C-17 is less enriched than the distal MEGT equivalents, suggesting that former is a better a correlative of MEGT/TM-19. The precisely defined geochemical correlations linking the Y-7 (Ionian Sea), PRAD-1870 (Adriatic Sea) and the ITS (Southern Tyrrhenian Sea) to the MEGT eruption reveal this to be one of the most widespread late Quaternary markers in the central Mediterranean region (Fig. 6) This is particularly important given its close stratigraphic association with the onset of MIS 3 and its potential to help asses spatial leads and lags in climate archives.

6.1.3 Volume and dispersal of MEGT tephra

The locations and thicknesses (where available) of distal MEGT tephra layers are shown in figure 6 and summarized in table 7. Ash produced during the MEGT eruption is confirmed as far as 540 km south-southeast of Ischia where it is recorded as the 4 cm thick Y-7 layer of the Ionian Sea (M25/4-11). This defines the major dispersal axis for this eruption. On the same axis, there are thicknesses of 20 cm in a southern Tyrrhenian Sea core (C-18, KET8003; Paterne et al., 1986) and 17 cm on Island of Stromboli (ITS). To the east, the MEGT tephra is 32 and 10 cm thick at LGdM and San Gregorio Magno, respectively, and is recorded as cryptotephras layers in central (PRAD 1870) and southern Adriatic cores (SA03-03; Bourne 2012). We have used these sites to make a preliminary estimate of the 25 and 4 cm isopach curves for MEGT tephra and envisage their dispersal axes. The 4 cm isopach curve has the same axis and elipticity as the 25 cm isopach, and passes through the Ionian Sea core site (Fig. 6).

We have used the isopach curves of figure 6 to provide a preliminary estimate of the volume of MEGT tephra deposited by particle fallout. It should be noted that this is a first order

estimate, both because the proximal volume is poorly constrained due to poor exposure on Ischia and because it is often not possible to distinguish between Plinian and co-ignimbrite fall in distal locations. The maximum thickness of MEGT fall deposits is 820 cm at Cavone dei Camaldoli on the southern side of Ischia (Brown et al., 2008). Assuming that the 25 and 4 cm isopach curves record deposition of tephra by fallout, then the MEGT tephra fall has a volume of ~40 km^3 using the Log Thickness vs. Square Root of the Area (Log *T* vs. $\sqrt{A}$) method of Pyle et al. (1989), modified by Fierstein and Nathenson (1992). When corrected for the lower density of fall deposits, this is in line with the ~15 km^3 estimate of total erupted magma determined from the size of the caldera (Brown et al., 2008).

6.1.4 Chronological constraints on the MEGT

The age of the MEGT eruption was determined on proximal rocks by K/Ar method at about 52 to 58 ka (Gillot et al. 1982). Distal equivalents of the MEGT have been directly dated by $^{40}Ar/^{39}Ar$, including the ITS layer dated at 56 ± 4 ka $^{40}Ar/^{39}Ar$ (Kraml 1997) and the LGdM TM-19 layer dated at 55 ± 2 ka (Watts et al., 1996). These proximal and distal ages are in good agreement, and the high-precision age of 55 ± 2 ka should be the preferred chronological constraint for the MEGT eruption and other distal equivalents. The $^{40}Ar/^{39}Ar$ age of the MEGT/TM-19 ash layer suggests that the LGdM calendar age determined for TM-19 (60,040 calendar yr BP) is an overestimate, indeed Wulf et al. (2012) recognised that section 5 (37,000-90,000 calendar yrs BP) in the LGdM record presents ca. 8% overestimate in calendar ages BP.

6.2 Proximal-LGdM tephra correlations

6.2.1 Pre-MEGT LGdM tephra correlations

6.2.1.1 TM-24-3b (104,020 varve yrs BP) and TM-23-20a (99.350 varve yrs BP)

These two tephras have glass compositions overlap with Pre-MEGT Group 2 glasses but extend to lower CaO (1.00 ± 0.04 wt%) (Fig. 7a) and Na_2O (7.8 ± 0.3 wt%), and higher SiO_2

(61.7 ± 0.5 wt%) contents. They have high incompatible element concentrations with (Fig.8 c,d). The glasses are displaced to lower ratios of HFSE to Th (i.e., Y/Th = 1.03 ± 0.05) relative to Pre-MEGT Group 2, and consequently form a new sub-parallel Pre-MEGT Group 3 trend (Fig, 7c-d) that is not known from the proximal stratigraphy. The compositional differences between TM-24-3b and TM-23-20a preclude correlations with the proximal pre-MEGT units studied here, disproving the proposed correlation between TM-24-3b and Sant'Angelo Tephra (Wulf et al., 2012). Thus the age of TM-24-3b should not be imported into the proximal stratigraphy.

6.2.1.2 TM-21-2a (80,990 varve yrs BP)

This layer, consistent with the Pre-MEGT Group 1a, extensively overlaps with the main Tisichiello glass population (Fig. 7), and has low statistical distance values (D^2_{majors} = 0.58 and D^2_{traces} = 1.20) on the basis of which a correlation cannot be excluded at 95% confidence limit. Figure 8c shows the chemical data of TM-21-2a tephra normalised to the average content of the Pre-MEGT Group 1a Tisichiello Tephra samples (OIS 0309 and OIS 0311). Whilst these samples are less evolved than the rest of the Tisichello tephra they represent the first erupted and coarsest pumice fall deposits of the Tisichello eruption and so may be more widely dispersed that the more evolved later products (OIS 0314 and OIS 0315). The LGdM tephra typically lies within 10% of the proximal Pre-MEGT sub-group 1a tephra for all major and trace elements. Therefore, we tentatively suggest a correlation between TM-21-2a and Tisichiello Tephra.

6.2.1.3 TM-20-5 (72,940 varve yrs BP)

This layer has Pre-MEGT Group 2 glass composition. Of the studied proximal glasses, TM-20-5 is most similar to that of the Olummo Tephra (D^2_{majors} = 0.59 and D^2_{traces} = 1.51), however small but significant systematic differences exist. TM-20-5 extends to lower CaO and MgO contents and its average HFSE concentrations that are consistently 5% lower

than Olummo values (Fig. 8b). Therefore, we do not correlate TM-20-5 with the proximal Olummo formation on Ischia. In fact, a TM-20-5-Olummo correlation would be inconsistent with the proposed link between the older LGdM TM-21-2a tephra and the overlying Tisichiello Tephra.

6.2.1.4 TM-20 (61,370 varve yrs BP), TM-20-1b (64,140 varve years BP) and TM-20-1c (64,470 varve yrs BP).

These three tephra layers have very similar Pre-MEGT Group 1b glass compositions (CaO <1.2 wt.% and MgO < 0.4 wt. % and exclusively $Na_2O > K_2O$) with limited compositional variation and thus are potential distal equivalents of the Porticello Tephra. A fourth LGdM layer, TM-20-1a (64.0 ka) was not analysed. The three studied distal tephras show extensive overlap with Porticello Tephra on all major and trace element biplots (Fig. 7). When compared to Porticello Tephra, calculated D^2 values are close to 1 for all three LGdM tephras (TM-20 $D^2_{major} = 0.87$, $D^2_{trace} = 1.16$; TM-20-1b $D^2_{major} = 1.06$, $D^2_{trace} = 0.46$; TM-20-1c $D^2_{major} = 0.81$, $D^2_{trace} = 0.87$), significantly below $D^2_{critical}$. Figure 8e-f shows that all three distal tephra generally lie within 10% of Porticello Tephra for all major and trace elements and fall within the envelope defined by the proximal Porticello Tephra glasses. However, this plot shows that, although concentrations of Rb, Zr, Nb, Ta, Th and U in TM-20 are within the concentration range defined by the proximal Porticello tephra, average concentrations of these elements are offset to 5% higher values. Therefore, we favour a correlation with TM-20-1b and/or TM-20-1c tephra. This correlation raises the possibility that the Porticello Tephra includes the deposits of more than one, but perhaps two closely spaced eruptions.

Previous distal-proximal correlations have linked tephra TM-20 with the Sant'Angelo Tephra of Ischia (Wulf et al., 2004). The Sant'Angelo Tephra deposits have Pre-MEGT Group 2 compositions (Table 4), in contrast to TM-20, TM-20-1b and TM-20-1c which all have a Pre-

MEGT Group 1a compositions. Therefore glass data presented herein does not support the previous correlations of TM-20 to the Sant'Angelo Tephra.

Previous distal-distal tephra correlations have linked LGdM tephra TM-20 with the distal marine tephra Y-7 (Wulf et al., 2004). Wulf et al., (2006) later proposed a correlation between LGdM tephras TM-20-1b and TM-20-1c and the Y-7 marine tephra. However, these correlations are not supported by our major and trace element glass data. The Y-7/MEGT tephra has Pre-MEGT Group 1a, Group 1b and Group 2 chemistries with both $Na_2O>K_2O$ and $K_2O>Na_2O$ and a wide ranging trace element concentrations (Zr 225-803 ppm, and Th 16-53 ppm), thus inconsistent with the TM-20, TM-20-1b and TM-20-1c glasses. Munno and Petrosino (2007) correlated the S-15 tephra recorded in the San Gregorio basin sequence to TM-20. However, as the S-15 tephra has $K_2O>Na_2O$, the correlation must be rejected on these grounds.

6.2.2 Post-MEGT LGdM tephra correlations

6.2.2.1 TM-18-17a (55,620 varve yrs BP)

This tephra layer is compositionally variable, with 1.3-1.8 wt% CaO, 61.7-62.8 wt% SiO_2 and K_2O/Na_2O ratios of 1.1-1.6 and low concentrations of incompatible trace elements (Th 13-24 ppm, Zr 204-360 ppm) falling into Post-MEGT Group 1. TM-18-17a shows a complete overlap with glasses from the Schiappone Tephra (Fig. 9a-d). The dominant population of LGdM tephra lies within 5% of the average composition of the least evolved glass in the Schiappone pumice fall deposit (SC-MEGT 0313) and ignimbrite (SC-MEGT 0315l) deposits of the Schiappone Tephra. A subordinate number of LGdM clasts extend to the less evolved compositions, and are within the envelope defined by the darker clasts in the PDC deposits (SC-MEGT 0315g) of the Schiappone Tephra (Fig. 9e). Therefore, we suggest that the Schiappone Tephra is the proximal equivalent of TM-18-17a layer.

Paterne et al. (1986) correlated the C-16 Tyrrhenian Sea tephra with the Upper Scarrupata di Barano Formation (Vezzoli 1988) on Ischia, these deposits have been subsequently included into the Schiappone Tephra (Brown et al., 2008). The following lines of evidence might support the existing correlation between Schiappone/TM-18-17a and C-16. C-16 chemical data presented by Paterne et al. (1986, 1988) from multiple cores show highly variable glass compositions with exclusively $K_2O>Na_2O$, consistent with those of the Schiappone Tephra. Concentrations of CaO are >1.3 wt% with a maximum of 2.5 wt%. This range is comparable to that displayed by proximal light and dark juvenile fragments of the Schiappone Tephra. Furthermore, bulk glass REE concentrations of C-16 overlap with the most evolved Schiappone glasses presented herein. Tyrrhenian Sea core tephra layer C-17, linked to MEGT by Paterne et al. (1986, 1988), is also a potential equivalent of Schiappone/TM-18-17a. The C-17 compositional data (Paterne et al. 1986) extend to higher (~1) K_2O/Na_2O values and lower (0.67-0.91 wt%) CaO content with overlapping REE concentrations. While a correlation between Schiappone/TM-18-17a and C-17 cannot be excluded, yet a C-16 tephra is a more convincing candidate on the basis of the available data.

6.2.2.2 TM-18-14a (50,260 varve yrs BP)

This tephra layer is compositionally variable, with concentrations of CaO ranging from 1.2 to 1.7 wt%, and SiO_2 from 61.7 to 62.9 wt%, and K_2O/Na_2O values between 0.9 and 1.5, and low to moderate incompatible trace element contents (Th 10.5-43.5 ppm, Zr 166-605 ppm). TM-18-14a is bimodal, the first population has CaO 1.31 ± 0.16 wt% and Th>35 ppm lie on the Post-MEGT Group 2 trend defined by the proximal deposits of the Pietre Rosse Tuff (Fig. 9a-d). The trace element composition of this TM-18-14a population is a good match for Pietre Rosse Tuff, falling within 10% of the average Pietre Rosse trace element composition (D^2_{trace} = 0.60). The major element composition of TM-18-14a is also a reasonable match (D^2_{major} = 1.77), however the CaO content is displaced to overlapping but higher CaO than

652 Pietre Rosse glasses (Fig. 8f). The second TM-18-14a population has Th<35 ppm fall on
653 the Post-MEGT Group 1 trend and extend to less evolved compositions (CaO 1.3-1.7 wt%,
654 Th 10-33 ppm, Zr 166-490 ppm). Whole-rock compositions comparable to this less evolved
655 TM-18-14a population are reported for Pietre Rosse Tuff by Civetta et al. (1991). We
656 suggest a correlation between TM-18-14a and Pietre Rosse given the good age and trace
657 element match, while noting a minor offset in major element composition.
658
659 *6.2.2.3 TM-18-9e (41,700 varve yrs BP)*
660 This tephra layer forms a cluster on major and trace element biplots with CaO = 1.28 ± 0.16
661 wt%, SiO_2 = 62.9 ± 0.5 wt% and K_2O/Na_2O = 1.0 ± 0.1. Incompatible element contents are
662 moderate (Th = 36 ± 2 ppm, Zr = 506 ± 37 ppm) and lie on post-MEGT trend 1 with high
663 incompatible element/Th. TM-18-9e glasses overlap with the proximal Agnone Tuff on major
664 and trace element biplots. The LGdM tephra TM-18-9e is offset to lower CaO (up to 30%)
665 and LREE-MREE (up to 20%) contents relative to Agnone Tuff. This is reflected in the
666 higher statistical distance values of D^2_{major} = 2.03 and D^2_{trace} = 9.57. Therefore, while we
667 cannot exclude a correlation between TM-18-9e and Agnone Tuff at 95% confidence, we do
668 not consider such a correlation to be likely.
669
670 6.2.2.4 TM-18-9a (41,420 varve yrs BP)
671 This tephra layer spans a narrow compositional range, with CaO 1.43 ± 0.07 wt% and
672 K_2O/Na_2O = 1.1 ± 0.1. TM-18-9a is a moderately evolved (Zr 335-454 ppm; Th 22-32 ppm)
673 Post-MEGT group 1 tephra that sits in the gap between Agnone and Pietre Rosse (Fig. 9a-
674 d) and does not correlate with any of the proximal units studied here.
675
676 *6.2.2.5 TM-17-1c (34,980 varve yrs BP)*
677 This tephra layer has two compositional modes. The dominant population has low CaO
678 (1.18 ± 0.05 wt%) and MgO (0.24 ± 0.02 wt%), high K_2O/Na_2O (0.89 ± 0.03) and moderate

679 incompatible element concentrations (Th = 43 ± 2 ppm; Zr = 582 ± 19 ppm and Nb = 91 ± 2
680 ppm) that lie in post-MEGT trend 2. This dominant TM-17-1c cluster overlaps extensively
681 with the proximal Pietre Rosse glass data (D^2_{major} = 1.49 and D^2_{trace} = 0.08). A second glass
682 population is similar in composition to the low-Th whole-rock composition reported for Pietre
683 Rosse Tuff by Civetta et al. (1991). Whilst chemically tephra TM-17-1c is also a good match
684 for Pietre Rosse, chronologically it is probably to young to represent the 46 ka (K-Ar) Pietre
685 Rosse (Civetta et al., 1991) thus we prefer a correlation with TM-18-14a. This emphasises
686 the importance of integrating chemical, stratigraphic and chronological information when
687 establishing proximal-distal correlations.
688
689 **6.2.3 Age constraints from proximal-LGdM tephra correlations**
690
691 In total, we define five proximal-LGdM tephra correlations on the basis of robust major and
692 trace element glass data: TM-21-2a/Tisichiello, TM-20-1b,c/Porticello, TM-19/MEGT, TM-
693 18-17a/Schiappone and TM-18-14a/Pietre Rosse (Fig. 10). These correlations allow ages
694 from the varved LGdM record to be imported into the proximal stratigraphy of Ischia. The
695 advantage of using the continuous chronostratigraphic record of LGdM is that it allows the
696 relative timing of closely-spaced eruptions to be resolved with a high degree of precision.
697 The absolute ages are overestimated by ca. 8% in the relevant section of the LGdM core
698 (section 5, 37,000-90,000 calendar yrs BP) as a result of incremental counting errors (Wulf
699 et al., 2012). However, the TM-19 layer has been directly dated by laser $^{40}Ar/^{39}Ar$ of
700 sanidine, giving an age of 55 ± 2 ka (Watts et al., 1996) for the MEGT. Therefore, we use
701 TM-19 as a chronological anchor for this portion of the LGdM record and then count varve
702 years from this independently dated tephra to generate more accurate ages for the
703 surrounding tephra layers. This works well for the Post-MEGT portion of the core giving
704 counting errors of ± 5%, but less well in the Pre-MEGT section where the core is not well
705 laminated and counting errors are closer to ±10%.

706

707 Applying the differential dating method to the Pre-MEGT, the correlation between Tisichiello
708 and TM-21-2a (80,990 varve years BP) implies an age of 76 ± 3 ka for the Tisichiello
709 eruption. Proximally, the Tisichiello deposits overlie the 74 ka Parata lava (Poli et al., 1987)
710 from which they are separated by Mago and Olummo tephra deposits. The Porticello
711 eruption is correlated with LGdM tephras TM-20-1b (64,140 varve years BP) and/or TM-20-
712 1c (64,470 varve yrs BP). The varve interval between TM-19 and TM-20-1c/TM-20-1b is
713 4080 and 3990 calendar years, giving a differential age of 59 ka ± 2 ka for the Porticello
714 tephra.

715

716 In the Post-MEGT time period, the age of TM-18-17a (*55,620 varve yrs BP*) gives an
717 differential age of 50.6 ± 2.0 ka for the voluminous Schiappone Tephra eruption. This is
718 consistent with the proximal K/Ar ages determined for the Schiappone Tephra, which are
719 generally 5 ka younger than the MEGT (Vezzoli, 1988; Brown et al., 2008). The Pietre
720 Rosse tephra is dated at 45 ± 2 ka by differential dating of LGdM tephra TM-18-14a (50,260
721 varve yrs BP). This is comparable to the K-Ar age of 46 ka reported by Civetta et al. (1991).

722

723 **7. Conclusions**

724 The largest known eruption of Ischia was the ~40 km^3, 55 ka MEGT, based on revised
725 proximal-distal tephra correlations we can extend the main south-south east dispersal to at
726 least 540 km. Distal equivalents of the MEGT occur in the Ionian (Y-7), Tyrrhenian (C-18),
727 and Adriatic (PRAD 1870) seas as well as at several locations in southern Italy. Thus, the
728 MEGT is one of the most widely dispersed late Quaternary tephras from the Campanian
729 region.

730

731 Tephra layers in the varved Lago Grande di Monticchio (LGdM) provide a valuable temporal
732 record of Ischia magmatism. The MEGT is correlated with TM-19 in LGdM, which has been

directly dated at 55 ± 2 ka (Watts et al., 1996). Differential dating, achieved by varve counting above and below the TM-19 tephra layer gives ages for LGdM tephra layers TM-21-2a (76 ± 3 ka), TM-20-1b,c (62-57 ka), TM-18-17a (50.6 ± 2.0ka) and TM-18-14a (45 ± 2 ka), which are correlated with Tisichiello, Porticello, Schiappone and Pietre Rosse, respectively. Previously suggested correlations between the Sant'Angelo tephra and TM-24-3b are not supported by our glass chemical data.

Proximal and distal LGdM tephra record a series of geochemical changes during the magmatic history of Ischia. Tephra compositions from the pre-MEGT (Sant'Angelo tephra to Porticello Tephra) period comprise three compositional groups that occur repeatedly in successive eruptions. Tephra from smaller eruptions (e.g. Sant'Angelo tephra and Porticello) contain just one group, while larger eruptions (e.g. Tisichiello and Olummo) record all three groups. Older tephra layers from LGdM (TM-24-3b and TM-23-20a) define a more evolved pre-MEGT compositional group not detected in the proximal rocks. Post-MEGT tephra (<55 ka) record a step to lower FeO and TiO_2 and form compositional groups that overlap with the pre-MEGT but are displaced to lower incompatible element contents. The repeated occurrence of glass compositions means that it is difficult to perform proximal-distal and distal-distal correlations for Ischia tephra without high quality major and trace glass data. This is particularly true for the smaller eruptions that typically show less compositionally variability.

Acknowledgements: This work is funded by the NERC RESET Consortium (NE/E015905/1). This is paper number ROX/0036. PA thanks Mauro Rosi for field guidance when sampling the Ischia tephra on Stromboli, Mark Hardiman is thanked for providing data for one LGdM tephra layer.

REFERENCES

Allen, Judy R M; Brandt, Ute; Brauer, Achim; Huntley, Brian; Keller, Jörg; Kraml, Michael;

760 Mackensen, Andreas; Mingram, Jens; Negendank, Jörg F W; Nowaczyk, Norbert R;
761 Watts, William A; Wulf, Sabine; Zolitschka, Bernd; Hubberten, Hans-Wolfgang;
762 Oberhänsli, Hedi (1999): Rapid environmental changes in southern Europe during
763 the last glacial period. *Nature*, 400 (6746**)**, 740-743
764 Bourne A. J., Lowe J. J., Trincardi F., Asioli A., Blockley S. P. E., Wulf S., Matthews I. P.,
765 Piva A. and Vigliotti L. (2010) Distal tephra record for the last ca 105,000 years from
766 core PRAD 1–2 in the central Adriatic Sea: implications for marine
767 tephrostratigraphy. Quaternary Sci. Rev. 29(23–24), 3079–3094.
768 Brauer, A., Allen, J.R.M., Mingram, J., Dulski, P., Wulf, S. and Huntley, B. (2007) Evidence
769 for last interglacial chronology and environmental change from Southern Europe.
770 Proc. Natl. Acad. Sci. U. S. A., 104 (2) 450-455.
771 Brown RJ, Orsi G, de Vita S (2008). New insights into Late Pleistocene explosive volcanic
772 activity and caldera formation on Ischia (southern Italy). Bulletin of Volcanology
773 70:583–603.
774 Brown RJ and Branney MJ, (2013) Internal flow variations and diachronous sedimentation
775 within extensive, sustained, density-stratified pyroclastic density currents flowing
776 down gentle slopes, as revealed by the internal architectures of ignimbrites on
777 Tenerife. Bulletin of Volcanology 75, 727
778 Brown, R.J, Civetta, L., Arienzo, I., D'Antonio, Moretti, R., Orsi, G., Tomlinson, E.L., Albert,
779 P.G., Menzies, M.A.. (2014) Geochemical and isotopic insights into the assembly,
780 evolution and disruption of a magmatic plumbing system before and after a
781 cataclysmic caldera collapse at Ischia volcano (Italy). Contributions to Mineralogy
782 and Petrology, 168, 1035 DOI 10.1007/s00410-014-10-
783 Bruno P, de Alteriis G, Florio G (2002) The western undersea section of the Ischia volcanic
784 complex (Italy, Tyrrhenian Sea) inferred by marine geophysical data. Geophys Res
785 Let 29: Art. No. 1343
786

787 Buchner G, Italiano A, Vita-Finzi C (1996) Recent upift of Ischia, Southern Italy. In: Jones,
788 W. J., Jones, A. P., and Neuberg, J. (Eds) Volcano instability on the Earth and other
789 planets, Geol Soc Spec Pub 110: 249–252
790 Calanchi N, Gasparotto G and Romagnoli C (1994) Glass chemistry in volcaniclastic
791 sediments of ODP Leg 107, Site 650, sedimentary sequence: provenance and
792 chronological implications. J. Volcanol. Geotherm. Res., 60, 59-85.
793 Cassidy, M., Watt, S. F.L., Palmer, M.R., Trofimovs, J., Symons, W., Maclachlan, S.E.,
794 Stinton, A.J (in press). Construction of volcanic records from marine sediment cores:
795 a review and case study (Montserrat, West Indies). Earth Science Reviews.
796 Civetta L, Gallo G, Orsi G (1991) Sr- and Nd-isotope and trace element constraints on the
797 chemical evolution of Ischia (Italy) in the last 55 ka. J Volcanol Geotherm Res 46:
798 213–230
799 Crisci GM, de Francesco AM, Mazzuoli R, Poli G, Stanzione D (1989) Geochemistry of the
800 recent volcanics of Ischia Island, Italy: evidences of crystallization and magma
801 mixing. Chem Geol 78: 15–33
802 D'Antonio M., Tonarini S., Arienzo I., Civetta L., Dallai L., Moretti R., Orsi G., Andria M.,
803 Trecalli A. - 2013 - Mantle and crustal processes in the magmatism of the Campania
804 region: inferences from mineralogy, geochemistry, and Sr-Nd-O isotopes of young
805 hybrid volcanics of the Ischia island (South Italy). Contr. Miner. Petrol., 165:1173-
806 1194, doi:10.1007/s00410-013-0853-x.
807 de Vita S, Sansivero F, Orsi G, Marotta E (2006) Cyclical slope instability and volcanism
808 related to volcano-tectonism in resurgent calderas: the Ischia island (Italy) case
809 study. Engen. Geol. 86: 148–165
810 Della Seta M., Marotta E., Orsi G., de Vita S., Sansivero F., Fredi P. - 2012 - Slope
811 instability induced by volcano-tectonism as an additional source of hazard in active
812 volcanic areas: the case of Ischia island (Italy): Bull. Volcanol., 74: 79-106,
813 doi:10.1007/s00445-011-0501-0.

814 Di Napoli R., Aiuppa A., Bellomo S., Brusca L., D'Alessandro W., Gagliano Candela E.,
815 Longo M., Pecoraino G., and Valenza M. (2009), A model for Ischia hydrothermal
816 system: Evidences from the chemistry of thermal groundwaters, J. Volcanol.
817 Geotherm. Res., 186, 133–159
818 Di Napoli R., Martorana R., Orsi G., Aiuppa A., Camarda M., De Gregorio S., Gagliano
819 Candela E., Luzio D., Messina N., Pecoraino G., Bitetto M., de Vita S., Valenza M. -
820 2011 - Highlights on the structure of hydrothermal systems from an integrated
821 geochemical, geophysical and geological approach: the Ischia Island case study.
822 Geochem. Geophys. Geosyst., 12, Q07017, doi:10.1029/2010GC003476.
823 Forcella F, Gnaccolini M, Vezzoli L (1982) I depositi piroclastici del settore sud-orientale
824 dell'isola d'Ischia (Italia). Riv It Paleaont Strat 89: 135–170
825 Gillot PY, Chiesa S, Pasquare G, Vezzoli L (1982) < 33 000 yr K/Ar dating of the volcano-
826 tectonic horst of the isle of Ischia, Gulf of Naples. Nature 229: 242
827 Hornig-Kjarsgaard, I., Keller, J., Koberski, U., Stadlbauer, E., Francalanci, L. & Lenhart, R.,
828 (1993): The Evolution of Stromboli Volcano.- In: Manetti, P. & Keller J. (Eds): The
829 island of Stromboli: Volcanic history and magmatic evolution.Acta Vulcanologica
830 3,21-68.
831 Keller J, Ryan WBF, Ninkovich D, Altherr R (1978) Explosive volcanic activity in the
832 Mediterranean over the past 200,000 yr as recorded in deep–sea sediments. Geol
833 Soc Am Bull 89: 591–604
834 Keller, J. (1969): Ritrovamenti di tufi alkali-trachitici della Campania nelle Isole Eolie.- Atti
835 Acc. Gioenia Catania, Ser. VII, Vol. I, 1-9.
836 Keller, J. (1981): Quaternary tephrochronology in the Mediterranean region.- NATO,
837 Advanced Study Institutes Series, Tephra Studies (S. Self & S. Sparks, Ed.), 227-
838 244.

839 Keller, J. (1994): Tephrochronology in the Ionian deep sea basin. In: Hieke, W., Halbach, P.,
840 Türkay, M. & Weikert, T. Mittelmeer 1993, Cruise No. 25 METEOR-Berichte 94-3,
841 165-167.
842 Keller, J., (1980) The island of Salina. Rendiconti della Società Italiana di Mineralogia e
843 Petrologia. 36, pp 489–524.
844 Kraml M. (1997) Laser-40Ar/39Ar-Datierungen an distalen marinen Tephren des jung-
845 quartären mediterranen Vulkanismus. Ph.D, Albert-Ludwigs-Universität Freiburg.
846 Lourens L.J. (2004) Revised tuning of Ocean Drilling Program Site 964 and KC01B
847 (Mediterranean) and implications for the $\delta^{18}O$, tephra, calcareous nannofossil, and
848 geomagnetic reversal chronologies of the past 1.1 Myr. Paleoceanography, 19(3),
849 DOI: 10.1029/2003PA000997
850 Lowe, J.J., et al., 2007. Age modelling of late Quaternary marine sequences in the Adriatic:
851 towards improved precision and accuracy using volcanic event stratigraphy.
852 Continental Shelf Research 27 (3–4), 560–582.
853 Lucchi, F., Tranne, C.A., De Astis, G, Keller, J., Losito, R., Morche, W (2008) Stratigraphy
854 and significance of Brown Tuffs on the Aeolian Islands (southern Italy). Journal of
855 Volcanology and Geothermal Research 177, 49–70.
856 Morche, W (1988) Tephrochronologie der Aolischen Inseln. PhD Thesis, Albert-Ludwigs-
857 Universitat Freiburg, Germany.
858 Moretti R., Arienzo I., Orsi G., Civetta L., D'Antonio M. - 2013 - The deep plumbing system
859 of the Ischia island (southern Italy): a physico-chemical and geodynamic window on
860 the fluid-sustained and CO_2-dominated magmatic source of Campanian volcanoes. J.
861 Petrol., 54 (5): 951-984.
862 Munno, R., Petrosino, P (2007) The late Quaternary tephrostratigraphical record of the San
863 Gregorio Magno basin (southern Italy). Journal of Quaternary Science. 22. 247-266.
864 Müller W., Shelley M., Miller P. and Broude S. (2009) Initial performance metrics of a new
865 custom-designed ArF excimer LA-ICPMS system coupled to a two-volume laser-

ablation cell. J. Anal. Atom. Spectrom. 24(2), 209–214.

Negri, A., Capotondi, L. & Keller, J. (1999): Calcareous nannofossils and planctonic foraminifera and oxygene isotopes in the late Quaternary sapropels of the Ionian Sea.- Marine Geol. 157, 89-103

Orsi G, Gallo G, Zanchi A (1991) Simple-shearing block resurgence in caldera depressions. A model from Pantelleria and Ischia. J Volcanol Geotherm Res 47: 1–11

Orsi G, Patella D, Piochi M, Tramacere A (1999) Magnetic modelling of the Phlegraean Volcanic District with extension to the Ponza archipelago, Italy. J Volcanol Geotherm Res 91: 345–360

Orsi G, Piochi M, Campajola L, D'Onofrio A, Gialanella L, Terrasi F (1996) 14C geochronological constraints for the volcanic history of the island of Ischia (Italy) over the last 5000 years. J Volcanol Geotherm Res 71: 249–257

Paterne M, Guichard F, Labeyrie J (1988) Explosive activity of the South Italian volcanoes during the past 80,000 years as determined by marine tephrochronology. J Volcanol Geotherm Res 34: 153–172

Paterne, M., Guichard, F., Labeyrie, J., Gillot, P. Y. & Duplessy, J. C. (1986) Tyrrhenian Sea tephrochronology of the oxygen isotope record for the past 60,000 years. Marine Geology 72, 259-285.

Pearce, N.J.G., Alloway, B.V., Westgate, J.A. 2008. Mid-Pleistocene silicic tephra beds in the Auckland region, New Zealand: Their correlation and origins based on trace element analyses of single glass shards. Quaternary International. 178, 16-43.

Perkins, M.E., Nash, W.P., Brown, F.H., Fleck, R.J., 1995. Fallout tuffs of Trapper Creek, Idaho: a record of Miocene explosive volcanism in the Snake River Plain volcanic province. Geological Society of America Bulletin 107 (12), 1484–1506.

Piochi M, Civetta L, Orsi G (1999) Mingling in the magmatic system of Ischia (Italy) in the past 5 ka. Min Pet 66: 227–258

892 Piva A, Asioli A, Schneider R, Trincardi F, Andersen N, Colmenero Hidalgo E, Dennielou B,
893 Flores J, Vigliotti L (2008) Climatic cycles as expressed in sediments of the
894 PROMESS1 borehole PRAD1-2, central Adriatic, for the last 370 ka: 1. Integrated
895 stratigraphy - art. no. Q01R01. Geochemistry Geophysics Geosystems, 9, DOI:
896 10.1029/2007GC001713
897 Poli S, Chiesa S, Gillot P–Y, Gregnanin A, Guichard F (1987) Chemistry versus time in the
898 volcanic complex of Ischia (Gulf of Naples, Italy): evidence of successive magmatic
899 cycles. Contrib Min Pet 95: 322–335
900 Pyle, DM (1989) The thickness, volume and grainsize of tephra fall deposits. Bull. Volcanol.,
901 51, 1-5
902 Rosi M, Sbrana A, Vezzoli L (1988) Correlazioni tefrostratigrafiche di alcuni livelli di Ischia,
903 Procida e Campi Flegrei. Mem Soc Geol It 41: 1015–1027
904 Sbrana A. (2009) Carta geologica d'Ischia, Foglio 464 Ischia (scale 1:10 000 CARG
905 Regione Campania)
906 Tamburrino (2008) Mediterranean tephrochronology: new insights from high-resolution
907 analyses of a 200,000 years long composite sedimentary log. Ph.D thesis, Universia
908 Degli Studi di Napoli “Frederico II”.
909 Tibaldi A, Vezzoli L (1998) The space problem of caldera resurgence: an example from
910 Ischia Island, Italy. Geol Rund 87: 53–66
911 Tomlinson E.L, Arienzo, I, Wulf S, Smith V.C, Carandente A, Civetta L, Hardiman M, Lane
912 C.S, Orsi G, Rosi M, Thirlwall M.T, Muller W and Menzies, M.A. (2012) Geochemistry
913 of the Phlegraean Fields (Italy) proximal sources for major Mediterranean tephras:
914 implications for the dispersal of Plinian co-ignimbritic components of explosive
915 eruptions. Geochim. et Cosmochim. Acta 93, 102-128
916 Tomlinson, E.L., Thordarson, T., Muller, W., Thirlwall, M., Menzies, M.A., 2010. Micro
917 analysis of tephra by LA-ICP-MS — strategies, advantages and limitations assessed
918 using the Thorsmork ignimbrite (Southern Iceland). Chemical Geology 279 (3–4), 73–

89.

Tonarini S., Leeman W. P., Civetta L., D'Antonio M., Ferrara G. and Necco A. (2004) B/Nb and systematics in the Phlegrean Volcanic District (PVD). J. Volcan. Geoth. Res. 113, 123–139.

Vezzoli L (Ed) (1988) Island of Ischia. Quaderni de La Ricerca Scientifica, Consiglio Nazionale delle Ricerca, Rome 114 pp.133

Vezzoli, L., Principe, C., Malfatti, J., Arrighi, S., Tanguy, J-C., Le Goff, M., Modes and times of caldera resurgence: The < 10 ka evolution of Ischia Caldera, Italy, from high-precision archaeomagnetic dating. J. Volcan. Geoth. Res. 186, 3-4, 305-319.

Watts, W.A., Allen, J.R.M., Huntley, B. (1996) Vegetation history and palaeoclimate of the last glacial period at Lago Grande di Monticchio, southern Italy. Quaternary Science Reviews 15, 133–153

Wulf S, Kraml M, Brauer A, Keller J, Negendank JFW (2004) Tephrochronology of the 100 ka lacustrine sediment record of Lago Grande di Monticchio (southern Italy). Quat Int 122: 7–30

Wulf, S., Brauer, A., Mingram, J., Zolitschka, B., Negendank, J.F.W (2006) Distal tephras in the sediments of Monticchio Marr lakes. In: Principe, C (E.d.), La geoligia del Mone Vulture. Regione Basilicata- Consiglio Nazionale delle Ricerche pp 105-122.

Wulf, S., Keller, J., Paterne, M., Mingram, J., Lauterbach, S., Opitz, S., Sottil, G., Giaccio, B., Albert, P.G., Satow, C., Tomlinson, E.L., Vicccaro, M., Brauer, A. (2012). The 100-133 ka record of Italian explosive volcanism and revised tephrochronology of Lago Grande di Monticchio. Quaternary Science Reviews, 58, 104-123.

Zembo I, Vignola P, Andò S, Bersezio R and Vezzoli L (2011). Tephrochronological study in the quaternary Val d'Agri intermontane basin (southern Apennines, Italy). Int. J. Earth Sci., 100, 173-187

Table captions

Table 1: Summary of proximal Ischia samples studied. Samples used in previous studies: 1 – Civetta et al. (1991); 2 – Brown et al. (2008). K-Ar ages are from *Gillot et al. (1982), $Vezzoli (1988) for units previously correlated with the MEGT) and §Poli et al. (1987). Mineral abbreviations: Alk fsp – alkali feldspar, bt – biotite, cpx – clinopyrxoene; plag – plagioclase, neph – nepheline.

Table 2: Summary of Lage Grande di Monticchio tephra layers studied. Varve ages are from Brauer et al. (2007). Mineral abbreviations: Alk fsp – alkali feldspar, bt – biotite, cpx – clinopyrxoene; plag – plagioclase, ac – acmite, ti – titanite, ap – apatite.

Table 3: Representative major (EMPA) and trace (LA-ICP-MS) element composition of proximal volcanic glass. Major elements are normalized to 100% and the analytical total given. The full dataset is given as online supplementary data.

Table 4: Geochemical groupings of the Pre-MEGT stratigraphy investigated on Ischia.. The sampled units follow the stratigraphy outlined in Brown et al. (2008; 2014).

Table 5: Geochemical groupings of the Post-MEGT stratigraphy investigated on Ischia. The sampled stratigraphic units follow the descriptions of Brown et al. (2008; 2014) and Civetta et al. (1991).

Table 6: Representative major (EMPA) and trace (LA-ICP-MS) element composition of Lago Grande di Monticcio tephra units. Major elements are normalized to 100% and the analytical total given. The full dataset is given as online supplementary data.

Table 7: Distal occurences of MEGT tephra used in volume calculation.

Figure captions

Figure 1: Sample localities: a) regional map showing the locations of Ischia and of the distal sample localities; b) Schematic map of Ischia showing the outcrop of rocks of different ages on the island (modified from Di Napoli et al., 2011; after Della Seta et al., 2011). And of proximal sample localities: 1 – Sant'Angelo peninsula; 2 – Grotta di terra; 3 – Cavone dei Camaldoli; 4 – Monte Vezzi; 5 – Monte Cotto; 6 – Citara Poseidon; 7 – Punta Imperatore (see figure 1 for sample locations).

Figure 2: Diagnositic major element glass data for investigated proximal units on Ischia spanning ~39-75 ka compared to the compositional fields of glass data sets from the other Neapolitan volcanic centres of Campi Flegrei (Tomlinson et al., 2012) and Vesuvius (Tomlinson et al., submitted). Errors are 2 s.d. calculated using replicate analyses of MPI-DING ATHO-G.

Figure 3: Major element biplots of proximal Ischia tephra from the Pre-MEGT (red, a-c), MEGT (green, d-f) and Post-MEGT (blue. G-i). Green field denotes MEGT composition. Errors are 2 s.d. calculated using replicate analyses of MPI-DING ATHO-G.

Figure 4: trace element biplots of proximal Ischia tephra from the Pre-MEGT (red, a-c), MEGT (green, d-f) and Post-MEGT (blue, g-i). Green field denotes MEGT composition. Errors are smaller than symbols and are calculated as 2 s.d. of replicate analyses of MPI-DING ATHO-G.

Figure 5: Biplots comparing potential distal correlatives of MEGT from the Tyrrhenian, Ionian and Adriatic sea and from the southern Italian mainland (see table 5 for references). Errors are 2 s.d. calculated using replicate analyses of MPI-DING ATHO, errors on trace element analyses are smaller than the data symbols.

Figure 6 Map showing locations and thicknesses (where available) of MEGT tephra and the inferred isopach thicknesses used for calculating the volume of MEGT tephra. Grey symbols indicate locations where chemical data is available, open symbols are locations oftephra correlated to Y-7, C-18 or MEGT but unconfirmed by this study (see table 5 for references).

Figure 7: Major and trace element biplots of Pre-MEGT tephra from Lago Grande di Monticchio (black symbols) compared to proximal Pre-MEGT tephra (red). Errors are 2 s.d. calculated using replicate analyses of MPI-DING ATHO-G, trace element errors are smaller than the data symbols.

Figure 8: Major and trace element compositions of LGdM tephra normalised to the average composition of the potential equivalent Pre-MEGT proximal tephra. The range of proximal compositions is given by the grey field. Plots exclude MnO, P_2O_5, which are close to the limit of detection and thus have poor precision in EMPA and also Sr and Ba, which are affected by microlite analysis in LA-ICP-MS.

Figure 9: (a-d) Major and trace element biplots of Post-MEGT tephra from Lago Grande di Monticchio (black symbols) compared to proximal Post-MEGT tephra (blue). Errors are 2 s.d. calculated using replicate analyses of MPI-DING ATHO-S. (e-f) Major and trace element compositions of LGdM tephra normalised to the average composition of the potential proximal Post-MEGT equivalent, the range of proximal compositions is given by the grey field. Plots exclude MnO, P_2O_5, which are close to the limit of detection and thus

have poor precision in EMPA and also Sr and Ba, which are affected by microlite analysis in LA-ICP-MS.

Figure 10: Correlations between the proximal Ischia stratigraphy (modified after Brown et al., 2008, K-Ar ages from Vezzoli 1988 and Poli et al. 1987) and the distal record at Lago Grande Di Monticchio (Wulf et al., 2004, 2012). Pre-MEGT tephra are in red, MEGT/TM-19 in green and post-MEGT in blue, with the youngest in light blue.

Eruption	*Age (ka)*	*Locality*	*Deposit description*	*Sample*	*Phenocrysts*	*Sample description*
Agnone	43[§]	Punta Imperatore	Pyroclastic pumicious tuff	OIS 103E[2]	Alk fsp , cpx, bt	Light grey, vesicular pumice
Pietre Rosse	46[§]	Citara Poseidon	Pyroclastic pumicious tuff	OIS 103F[2]	Alk fsp , bt	White, vesicular pumice
Schiappone	50[$]	Monte Cotto Monte Vezzi	6m thick pumice fall overlain by >60m thick ignimbrite	SC-MEGT 0315 (light and dark clasts from ignimbrite)[3] SC-MEGT 0313 (fall)[1] SC MEGT 0309	Alk fsp, plag, bt, cpx	White to grey, vesicular pumice
MEGT	51-59*	Acquamorta Cavone dei Camaldoli	Extracaldera ignimbrite 0.5 m thick Extracaldera deposit comprising 8.5m basal fall overlain by 3.5 welded ignimbrite and capped by a lithic breccia	CF 191 (ignimbrite)[4] OIS 0319 (breccia)[3] OIS 0325 (ignimbrite)[1] OIS 0333 (fall)[3] OIS 0321 (fall)[1]	Alk fsp, cpx, bt	Green to grey vesicular pumice Light to dark grey vesicular pumice Grey, poorly vesiculated pumice Orange/ buff coloured vesicular pumice Light-grey vesicular pumice
Porticello	-	Grotta di Terra	<4m thick deposit of pumice fall with thin ash beds	OIS 0320 (fall)[1] OIS 0316 (fall)[3]	Alk fsp, cpx, bt	Buff coloured vesicular pumice
Tisichiello	-	Grotta di Terra	7m thick sequence of interbedded pumice fall and ash-rich pyroclastic density currents.	OIS 0315 (fall)[3] OIS 0314 (fall)[3] OIS 0311 (fall)[3] OIS 0309 (fall)[1]	Alk fsp, plag, cpx, bt	Buff coloured vesicular pumice
Olummo	-	Grotta di Terra	6m thick sequence of interbedded pumice fall deposits and thin ash beds overlain by block and ash flow deposit	OIS 0318 (block and ash)[3] OIS 0305 (fall)[3] OIS 0302 (fall)[1]	Alk fsp, plag, cpx, bt	Buff to Light grey coloured vesicular pumices
Sant'Angelo	-	Sant' Angelo peninsula	Interbedded pumice fall deposits and thin ignimbrites overlain by thick lithic breccia.	OIS 0330 (Ignimbrite)[3] OIS 0326 (fall)[1]	Alk fsp, cpx, bt, neph,	Buff to light grey coloured vesicular pumices

Table 1

Tephra	Depth (cm)	Varve Age (Cal BP)	Thickness (mm)	Max grain size (µm)	Colour	Phenocrysts	Lithics
TM-17-1c	2372.8	34980	5	100	white	Kf, plg, cpx, bt	V
TM-18-9a	2992.0	41420	1.5	500	white-beige	Kf, cpx, bt, plg, ap	V
TM-18-9e	3005.2	42000	13	200	white-beige	Kf, plg, bt, cpx	V
TM-18-14a	3345.4	50260	1	700	grey-brown	Kf, plg, cpx, bt	V
TM-18-17a	3508.5	55620	5	400	beige	Kf, cpx, plg, bt	-
TM-19	3831.0	60060	332	1100	beige-green	Kf, bt, cpx, plg	V
TM-20	3923.8	61370	6	200	beige	Kf, bt, plg, cpx, ac, ti	V
TM-20-1b	4067.6	64140	8	300	beige	Kf, bt, cpx, plg, ap	V
TM-20-1c	4104.7	64470	3	230	grey-brown	Kf, bt, cpx, ap, ac	V
TM-20-5	4657.0	72940	20	150	beige	Kf, cpx, bt, plg	V
TM-21-2a	5236.2	80990	7.5	200	white	Plg, kf, cpx, bt, ap	V
TM-23-20a	6685.9	99140	24	310	white-ockre	Kf, plg, bt, cpx	V
TM-24-3b	7243.6	103800	8	190	white	Kf, plg, cpx, bt, ap	-

Table 2

	Agn-one	Pietre Rosse	Schiappone		MEGT			Porti-cello	Tisichiello			Olummo			Sant'Angelo	
Analysis	OIS 103E-18	OIS 103F-17	SC-MEGT 0315l-1	SC-MEGT 0315g-15	OIS 0333-16	CF 319-6	OIS 0333-16	OIS 0320-6	OIS 0311-20	OIS 0315-9	OIS 0314-21	OIS 0302-6	OIS 0305-25	OIS 0318-28	OIS 0326-5	OIS 0330-3
Total	95.63	94.73	94.27	96.79	96.15	95.83	96.15	95.44	95.57	97.99	96.59	96.81	93.53	93.46	96.51	96.10
SiO_2	62.87	62.63	62.03	60.11	62.15	62.55	62.64	61.81	61.83	61.67	61.54	60.85	62.14	61.93	61.95	61.75
TiO_2	0.56	0.46	0.50	0.55	0.50	0.49	0.62	0.56	0.55	0.58	0.52	0.61	0.49	0.62	0.65	0.56
Al_2O_3	18.35	18.37	18.42	18.84	18.24	18.22	18.71	18.75	18.80	18.75	18.29	18.77	18.44	18.74	18.69	18.44
FeO	2.47	2.27	2.40	3.62	2.60	2.72	2.34	2.51	2.56	2.73	2.75	2.80	2.51	2.75	2.36	2.68
MnO	0.19	0.23	0.18	0.15	0.24	0.08	0.25	0.29	0.14	0.29	0.33	0.32	0.19	0.18	0.22	0.26
MgO	0.33	0.24	0.30	0.80	0.30	0.54	0.24	0.28	0.36	0.35	0.25	0.28	0.40	0.51	0.39	0.36
CaO	1.33	1.18	1.40	2.52	0.74	1.53	0.88	1.12	1.31	1.15	0.99	1.02	1.32	1.30	1.24	1.09
Na_2O	6.44	7.45	6.78	4.94	8.22	5.72	8.03	7.26	6.91	7.19	8.51	8.49	7.01	6.49	7.22	7.91
K_2O	6.79	6.42	7.39	7.96	6.15	7.77	5.77	6.68	6.92	6.53	5.92	6.00	6.87	6.91	6.64	6.16
P_2O_5	0.06	0.04	0.07	0.17	0.03	0.12	0.04	0.05	0.10	0.09	0.04	0.09	0.05	0.07	0.03	0.09
Cl	0.62	0.71	0.53	0.35	0.83	0.27	0.49	0.69	0.51	0.68	0.85	0.77	0.58	0.51	0.60	0.71
V	32	23	36	79	25	42	25	27	31	31	23	28	25	28	33	25
Rb	422	343	334	247	516	259	516	526	310	459	550	570	539	245	482	531
Sr	4.4	<LOD	20.6	392	<LOD	36	<LOD	10.4	15.5	10.2	1.7	2.3	5.3	135	10.4	3.1
Y	51	48	38	24	72	25	72	73	39	63	73	90	75	29	70	70
Zr	503	576	369	210	796	202	796	693	381	638	947	1057	887	305	875	761
Nb	85	91	60	35	123	38	123	111	64	106	143	158	147	49	123	124
Ba	3.6	<LOD	10.3	661	3.8	31.2	4	3.3	7.9	13.1	2.3	3.3	4.6	121	6.9	3.2
La	107	109	80	53	157	60	157	146	87	131	168	201	175	74	163	156
Ce	216	202	158	104	301	117	301	296	185	265	321	372	333	135	311	298
Pr	24	20	17	11	30	13	30	32	18	28	33	37	33	14	31	30
Nd	88	73	58	43	102	48	102	115	66	99	104	118	111	47	106	105
Sm	16.2	11.9	10.0	8.5	17.1	<LOD	17.1	22.0	11.0	17.8	14.5	19.8	21.9	8.6	16.6	17.4
Eu	1.4	0.9	1.4	1.9	1.0	1.5	1.0	<LOD	1.3	1.3	0.9	1.0	<LOD	1.9	1.1	0.9
Gd	12.5	8.8	9.2	6.1	12.6	6.9	12.6	13.4	9.0	13.0	12.8	14.4	13.4	6.2	13.3	12.2
Dy	10.2	8.0	7.0	4.8	11.8	5.1	11.8	13.5	7.9	11.3	11.8	13.9	13.5	5.3	11.9	11.7
Er	5.2	5.2	3.9	2.4	7.7	2.7	7.7	7.7	4.2	6.6	7.4	9.1	7.5	2.9	7.0	6.8
Yb	5.4	5.5	4.2	2.5	8.3	2.6	8.3	6.7	3.8	6.4	7.5	10.3	7.4	3.0	7.0	7.3
Lu	0.8	0.9	0.6	<LOD	1.1	<LOD	1.1	0.9	0.6	1.0	1.1	1.4	1.3	0.4	1.2	1.1
Ta	4.4	4.2	3.2	1.7	5.7	1.9	5.7	5.7	3.0	5.0	5.7	6.6	5.9	2.4	5.7	5.5
Th	38	43	22.7	13.1	52	14.1	52	45	26	42	59	78	60	20	61	52
U	13.0	14.2	7.8	4.6	15.7	4.3	15.7	14.1	7.9	13.3	18.0	23.1	18.1	6.3	18.0	16.1

Table 3

Stratigraphic order of sampled units

Tephra	Chemical Groupings
Pre-MEGT Stratigraphy	**Pre-MEGT Groups**
Porticello Tephra	
OIS 0320 (fall	Pre-MEGT Group 1b
OIS 0316 (fall)	
Tisichiello Tephra	
OIS 0315 (fall)	Pre MEGT Group 1b and 2
OIS 0314 (fall)	
OIS 0311 (fall)	Pre-MEGT Group 1a
OIS 0309 (fall)	
Olummo Tephra	
OIS 0318 (block and ash)	Pre-MEGT Group 1a
OIS 0305 (fall)	Pre-MEGT Group 1b and 2
OIS 0302 (fall)	Pre-MEGT Group 2
Sant'Angelo Tephra	
OIS 0330 (flow)	Pre-MEGT Group 2
OIS 0326 (fall)	

Table 4

Stratigraphic order of sampled units

Tephra	Chemical Groupings
Post-MEGT Stratitgraphy	**Post-MEGT Groups**
Agnone Tuff	
OIS 103E-2	Post-MEGT Group 1
Pietre Rosse Tuff	
OIS 103F[2]	Post-MEGT Group 2
Schiappone Tephra	
SC-MEGT 0315 (light and dark clasts from ignimbrite)[3]	Post-MEGT Group 1
SC-MEGT 0313 (fall)[1]	
SC MEGT 0309 (fall)	

Table 5

LGdM layer	TM-17-1c	TM-17-1c	TM-18-9a	TM-18-9a	TM-18-9e	TM-18-14a	TM-18-14a	TM-18-14a	TM-18-17a	TM-18-17a	TM-19	TM-19	TM-19	TM-19	TM-20	TM-20-1b	TM-20-1c	TM-20-5	TM-21-2a	TM-23-20a	TM-24-3b
analysis	15	20	1	7	6	11	9	17	19	17	14	20	43	25	3	1	8	7	2	14	13
sum	90.84	94.03	93.91	95.34	98.16	92.28	93.06	96.81	92.56	93.49	96.14	98.08	96.77	95.97	94.89	95.71	99.83	99.12	96.60	98.35	97.64
SiO_2	62.44	62.88	63.38	62.98	63.04	62.35	62.57	62.32	62.72	62.13	62.05	61.75	61.97	62.64	62.05	62.35	61.96	61.34	62.49	61.84	62.08
TiO_2	0.44	0.48	0.43	0.50	0.46	0.42	0.47	0.41	0.42	0.44	0.57	0.59	0.55	0.56	0.62	0.60	0.61	0.57	0.55	0.57	0.71
Al_2O_3	18.46	18.34	18.47	18.65	18.20	18.74	18.63	18.44	18.44	18.57	18.48	18.44	18.61	18.26	18.62	18.47	18.41	18.58	18.46	18.46	18.07
FeO	2.54	2.30	2.28	2.37	2.23	2.26	2.26	2.71	2.24	2.56	2.69	2.62	2.61	2.45	2.61	2.49	2.56	2.75	2.65	2.68	2.85
MnO	0.13	0.27	0.16	0.13	0.11	0.17	0.13	0.13	0.22	0.07	0.22	0.23	0.25	0.21	0.28	0.22	0.23	0.26	0.20	0.30	0.31
MgO	0.48	0.25	0.26	0.29	0.24	0.27	0.27	0.43	0.30	0.48	0.33	0.30	0.30	0.42	0.29	0.27	0.29	0.29	0.36	0.30	0.33
CaO	1.65	1.19	1.35	1.42	1.27	1.36	1.38	1.72	1.40	1.81	1.12	1.12	0.99	1.30	1.08	1.08	1.11	0.97	1.31	0.99	0.97
Na_2O	5.33	7.19	5.78	6.06	6.87	7.12	6.46	5.42	6.38	5.23	7.57	7.86	7.77	6.84	7.37	7.24	7.55	8.49	6.37	7.96	7.87
K_2O	8.07	6.36	7.31	6.96	6.84	6.50	7.06	7.95	7.25	8.17	6.14	6.27	6.20	6.66	6.32	6.51	6.59	5.90	7.07	5.99	6.01
P_2O_5	0.09	0.05	0.04	0.06	0.02	0.09	0.04	0.09	0.05	0.13	0.05	0.05	0.05	0.08	0.05	0.06	0.04	0.03	0.04	0.03	0.03
Cl	0.36	0.70	0.55	0.59	0.71	0.71	0.72	0.37	0.59	0.40	0.78	0.75	0.69	0.57	0.71	0.70	0.63	0.82	0.51	0.87	0.77
V	45	25	26	36	26	28	32	45	35	49	28	25	32	35	28	27	26	23	33	<LOD	<LOD
Rb	260	447	343	349	388	422	375	252	322	255	503	424	360	286	474	444	458	551	314	553	540
Sr	100.2	4.1	16.5	24.7	4.9	13.8	9.6	101.3	23.7	99.7	4.4	3.8	6.0	15.5	4.1	6.0	3.0	2.1	<LOD	<LOD	<LOD
Y	24	51	31	40	48	44	42	26	35	25	68	67	45	30	63	63	65	75	43	78	76
Zr	217	599	335	419	500	557	452	222	345	219	789	645	391	258	651	605	612	875	407	1024	946
Nb	38	92	59	67	81	88	77	37	56	36	123	110	71	46	110	104	107	136	67	144	144
Ba	81.4	9.2	15.1	24.9	2.2	13.2	9.3	83	18.9	78	12.0	11.1	5.1	10.8	4.8	7.4	3.7	5.2	<LOD	<LOD	8.9
La	53	116	69	86	100	109	90	55	76	55	149	129	92	68	138	127	134	164	92	182	193
Ce	103	216	133	167	195	205	177	107	150	108	290	258	189	135	265	260	272	321	184	327	355
Pr	11	21	14	18	20	20	18	12	15	11	30	28	20	14	28	27	28	30	19	31	34
Nd	41	70	49	63	70	67	67	43	60	41	102	102	75	55	98	95	96	104	71	101	114
Sm	7.3	11.9	<LOD	11.8	12.1	12.2	12.0	8.1	10.1	7.1	17.2	20.4	16.4	10.6	16.7	16.2	16.9	16.4	<LOD	15.4	17.1
Eu	1.6	<LOD	<LOD	1.4	1.1	<LOD	1.2	1.5	1.3	1.6	0.9	0.9	1.3	1.3	1.0	1.0	1.2	0.9	<LOD	<LOD	<LOD
Gd	5.6	8.6	<LOD	8.2	9.5	8.6	9.3	6.0	8.0	5.7	13.8	12.4	10.4	6.7	12.3	12.2	12.0	14.6	<LOD	11.6	13.3
Dy	4.5	8.5	5.8	7.3	8.1	8.1	7.6	5.1	6.9	4.5	12.5	11.8	8.1	6.4	12.1	11.4	11.8	12.8	<LOD	11.3	12.5
Er	2.5	5.2	3.1	4.0	4.7	4.6	4.0	2.6	3.5	2.6	6.8	6.2	4.6	3.2	6.7	6.1	6.5	7.0	<LOD	7.9	7.7
Yb	2.5	5.7	3.3	4.1	4.9	5.2	4.5	2.7	3.6	2.1	8.0	5.4	4.0	3.0	6.9	6.1	6.6	7.8	<LOD	8.1	8.7
Lu	<LOD	0.8	<LOD	0.6	0.8	0.8	0.7	<LOD	0.5	0.4	1.0	0.9	0.6	0.4	1.0	0.9	1.0	1.1	<LOD	<LOD	<LOD
Ta	1.9	4.0	2.9	3.6	4.3	4.3	3.6	2.0	2.8	1.8	5.5	5.4	3.6	2.5	5.4	5.1	5.1	6.0	<LOD	5.9	6.2
Th	14	44	22	30	35	38	30	15	22	14	53	37	27	18	45	41	43	59	28	69	76
U	4.5	13.8	7.8	9.2	11.7	12.7	9.9	4.5	6.8	4.1	15.8	11.6	7.4	5.3	14.0	12.5	12.7	19.1	8.5	24	23

Site	Location	Layer	Thickness (cm)	Direction	Reference
Core					
PRAD 1-2	Adriatic sea	1870 cm	crypto	NNE	Bourne et al, 2010
KET 82-18	Adriatic sea	C-18	unknown	ENE	Paterne et al., 1988
M25/4-11	Ionian Sea	Y-7	4cm	SE	Keller et al., 1994, 1978; Kraml 1997
M25/4-10	Ionian Sea	Y-7	>2cm[§]	SE	Keller et al., 1994
M25/4-12	Ionian Sea	Y-7	3.5-4 cm	SE	Keller et al., 1994
M25/4-13	Ionian Sea	Y-7	4.5 cm	SE	Keller et al., 1994
RC9-190	Ionian Sea	Y-7	unknown	SE	Keller et al., 1978
RC9-191*	Ionian Sea	Y-7	unknown	SE	Keller et al., 1978
V10-68	Ionian Sea	Y-7	unknown	SE	Keller et al., 1978
KC01B	Ionian Sea	tephra 14	unknown	SE	Lourens, 2004
KET 8003*	Tyrrhenian Sea	C-18	unknown	SSE	Paterne et al., 1988
KET 8011	Tyrrhenian Sea	C-18	unknown	S	Paterne et al., 1988
MD01_2474G	Tyrrhenian Sea	MD28	11	S	Tamburrino, 2008
ODP Leg 107-650*	Tyrrhenian Sea	T003	3.5	S	Calanchi et al. 1994, McCoy and Cornell 1990
KET 8004*	Tyrrhenian Sea	C-18	20	SSW	Paterne et al., 1986, 1988
KET 8022*	Tyrrhenian Sea	C-18	unknown	W	Paterne et al., 1988
Lago Grande di Monticchio	Southern Italy	TM-19	32 (2 cm fall)	E	Wulf et al., 2004
San Gregorio Magno*	Southern Italy	S16	10	E	Munno and Petrosino 2007
Outcrop					
Val d'Agri	Southern Italy	T3D4	18	ESE	Zembo et al., 2011
Stromboli	Aeolian Islands	IT	25-30	SSE	Morche 1988, Hornig- Kjarsgaard et al. 1993
Salina*	Aeolian Islands	IT	35-40	SSE	Keller 1969
Lipari	Aeolian Islands	IT	30-50	S	Lucchi et al 2008
Panarea	Aeolian Islands	IT	17	S	Lucchi et al 2008
Filicudi	Aeolian Islands	IT	30-50	S	Lucchi et al 2008

Bold, chemical data available (*major element only)
[§]core is cut through this layer so 2 cm is a minimum.

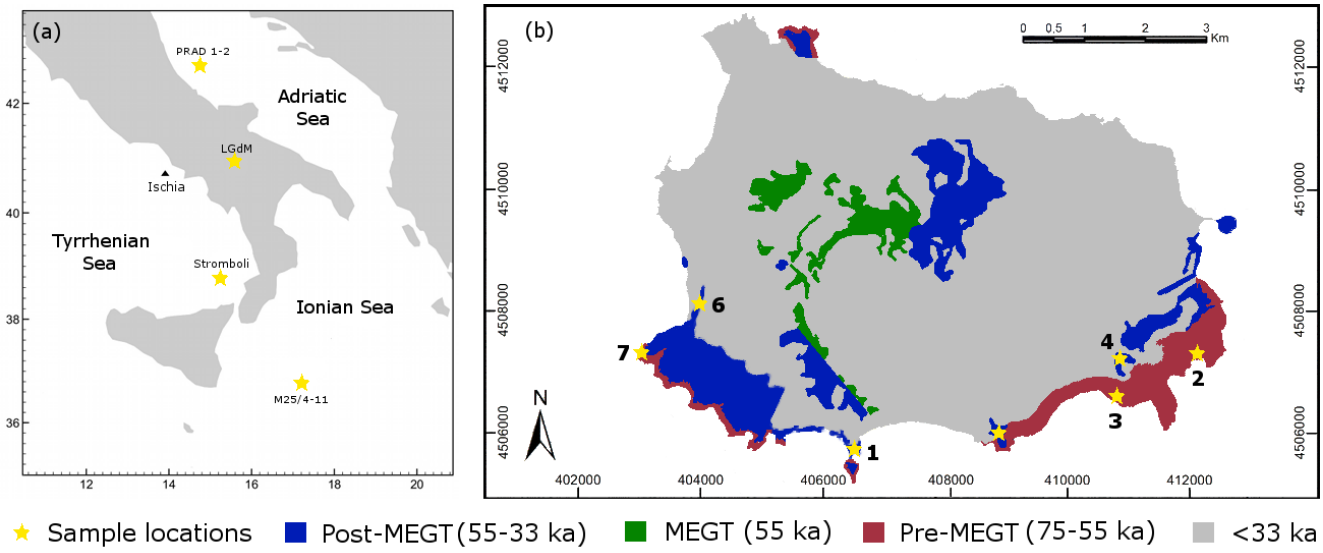
(a)
PRAD 1-2
Adriatic Sea
LGdM
Ischia
Tyrrhenian Sea
Stromboli
Ionian Sea
M25/4-11
(b)
0 0.5 1 2 3 Km
N
1
2
3
4
6
7
Sample locations
Post-MEGT (55-33 ka)
MEGT (55 ka)
Pre-MEGT (75-55 ka)
<33 ka

Fig 1

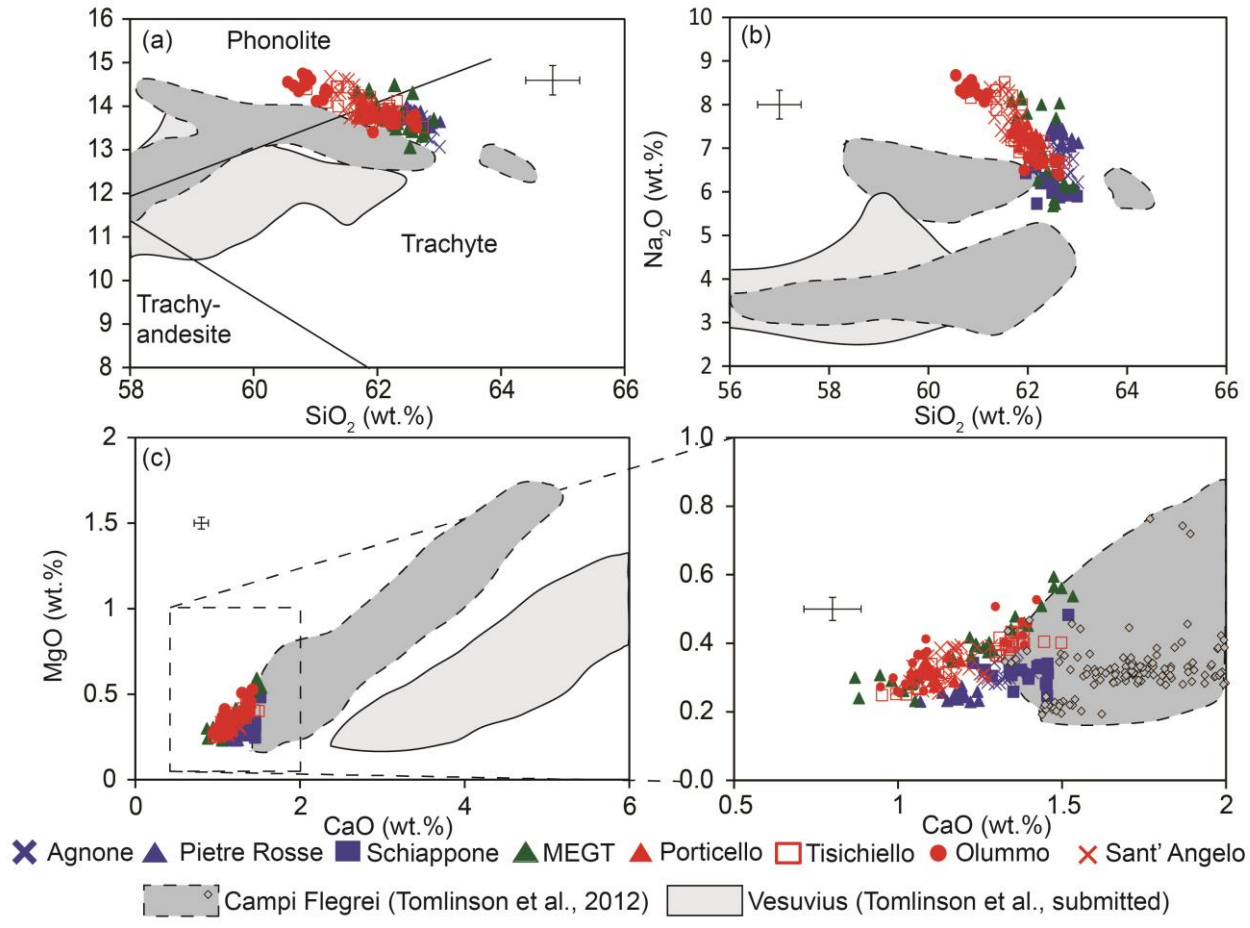
(a)
Phonolite
Trachyte
Trachy-andesite
SiO2 (wt.%)
(b)
Na2O (wt.%)
SiO2 (wt.%)
(c)
MgO (wt.%)
CaO (wt.%)
CaO (wt.%)
Agnone
Pietre Rosse
Schiappone
MEGT
Porticello
Tisichiello
Olummo
Sant' Angelo
Campi Flegrei (Tomlinson et al., 2012)
Vesuvius (Tomlinson et al., submitted)

Fig 2

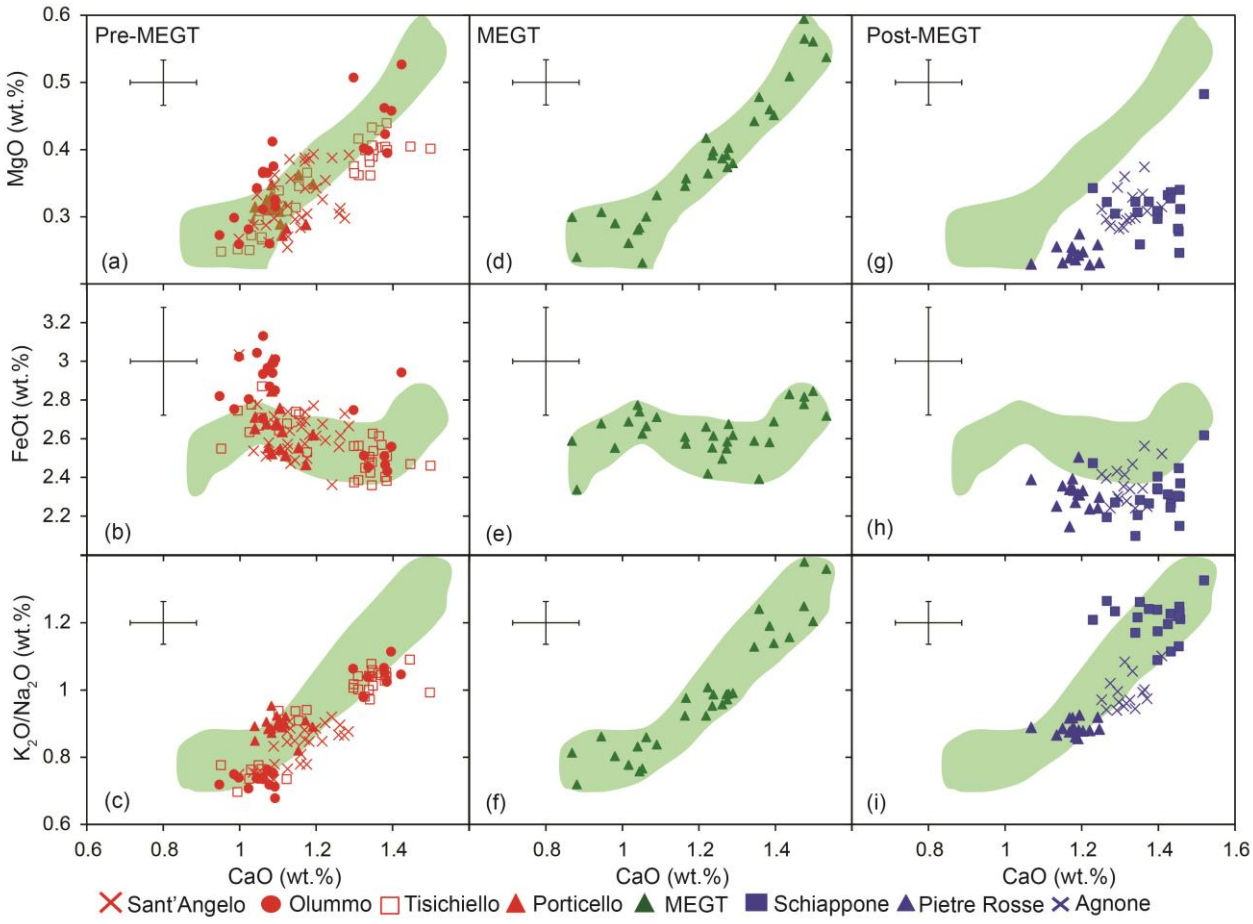
Pre-MEGT
MEGT
Post-MEGT
MgO (wt.%)
FeOt (wt.%)
K2O/Na2O (wt.%)
CaO (wt.%)
(a)
(b)
(c)
(d)
(e)
(f)
(g)
(h)
(i)
Sant'Angelo
Olummo
Tisichiello
Porticello
MEGT
Schiappone
Pietre Rosse
Agnone

Fig 3

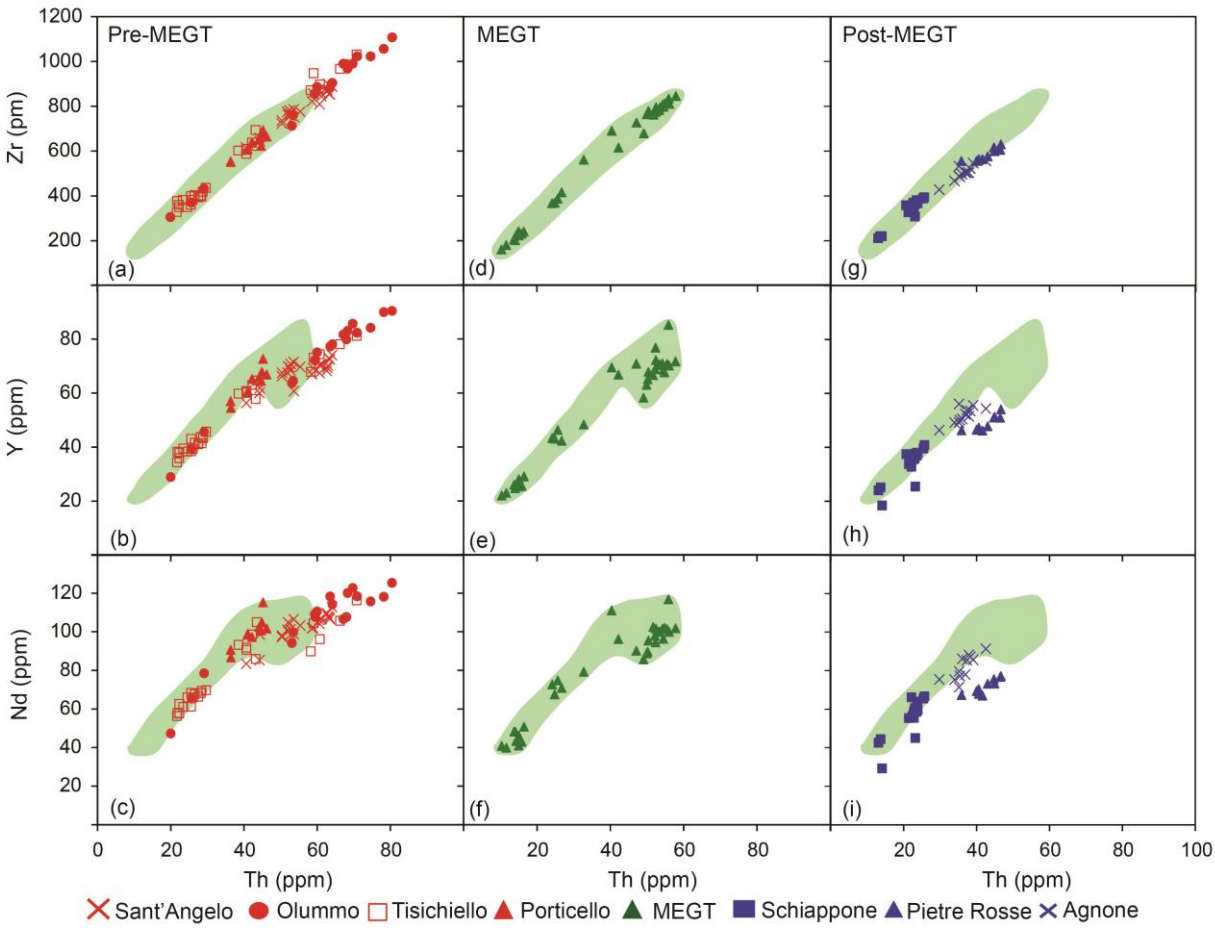
Pre-MEGT
MEGT
Post-MEGT
Zr (ppm)
Y (ppm)
Nd (ppm)
Th (ppm)
(a)
(b)
(c)
(d)
(e)
(f)
(g)
(h)
(i)
Sant'Angelo
Olummo
Tisichiello
Porticello
MEGT
Schiappone
Pietre Rosse
Agnone

Fig 4

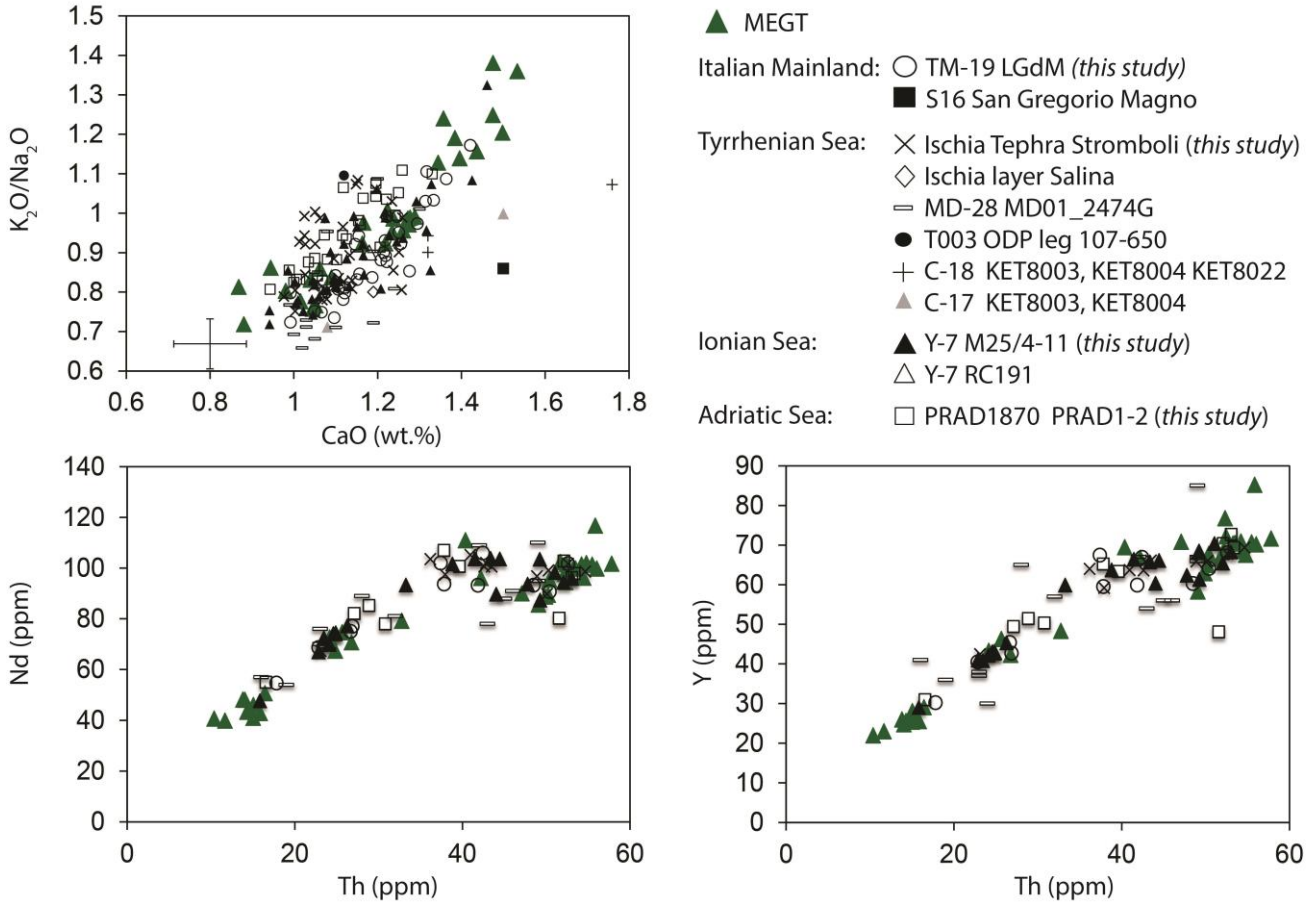
MEGT
Italian Mainland:
TM-19 LGdM (this study)
S16 San Gregorio Magno
Tyrrhenian Sea:
Ischia Tephra Stromboli (this study)
Ischia layer Salina
MD-28 MD01_2474G
T003 ODP leg 107-650
C-18 KET8003, KET8004 KET8022
C-17 KET8003, KET8004
Ionian Sea:
Y-7 M25/4-11 (this study)
Y-7 RC191
Adriatic Sea:
PRAD1870 PRAD1-2 (this study)
K2O/Na2O
CaO (wt.%)
Nd (ppm)
Th (ppm)
Y (ppm)
Th (ppm)

Fig. 5

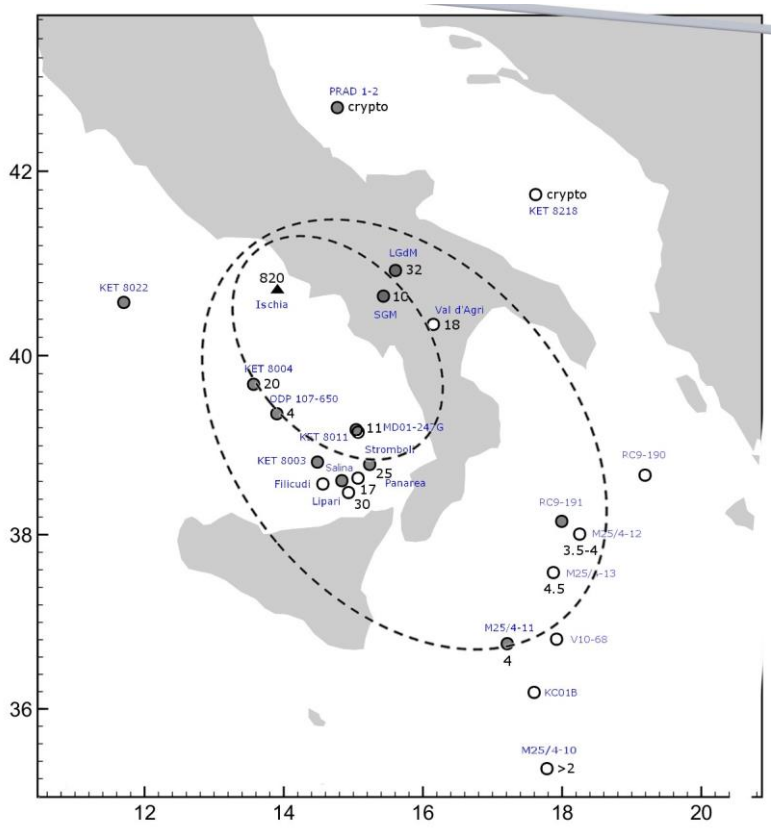
PRAD 1-2
crypto
crypto
KET 8218
LGdM
32
820
Ischia
10
SGM
Val d'Agri
18
KET 8022
KET 8004
20
ODP 107-650
4
11
MD01-247G
KET 8011
Stromboli
KET 8003
Salina
25
Filicudi
Panarea
17
Lipari
30
RC9-190
RC9-191
M25/4-12
3.5-4
M25/4-13
4.5
M25/4-11
4
V10-68
KC01B
M25/4-10
>2
42
40
38
36
12
14
16
18
20

Fig 6

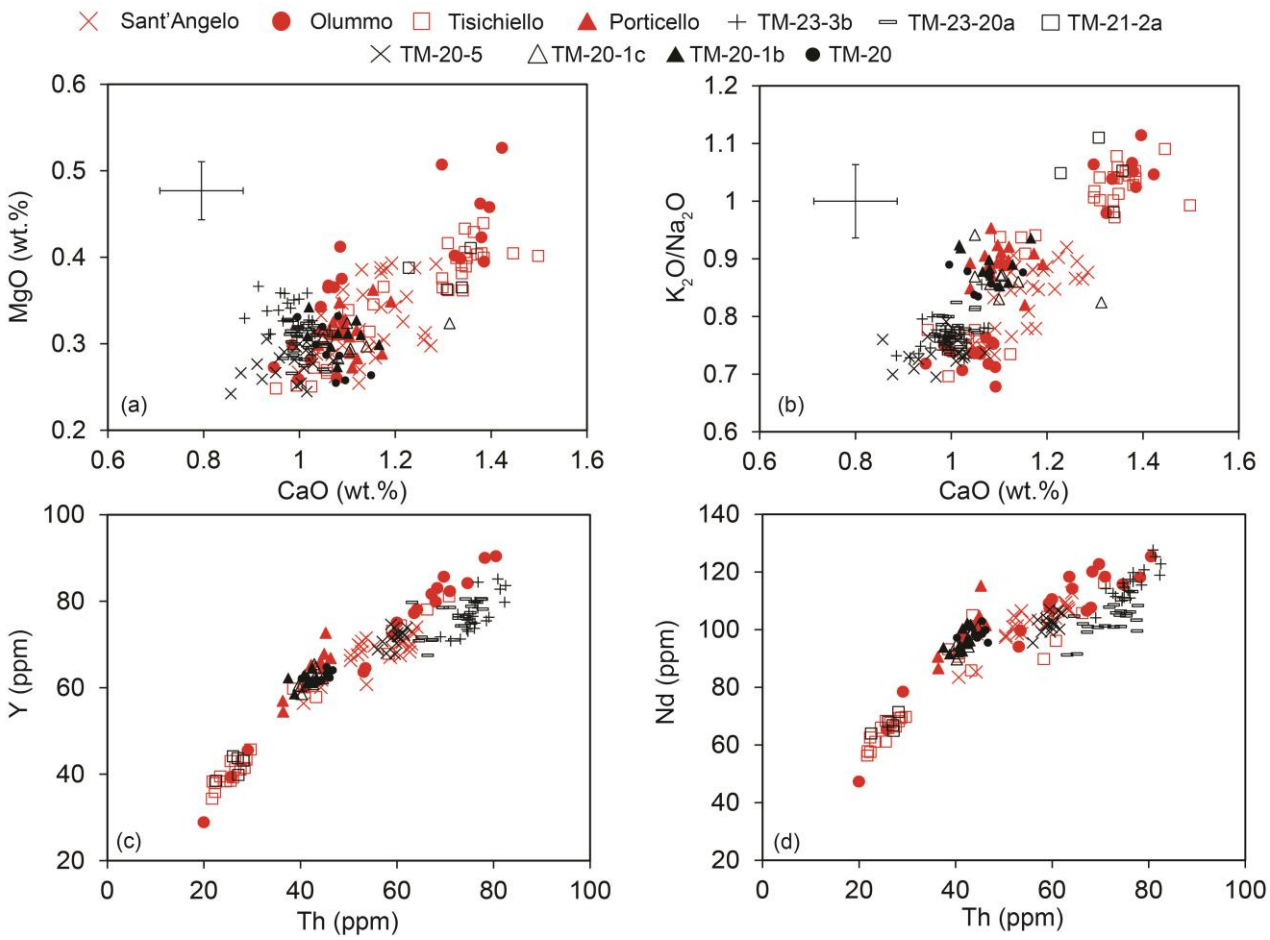
Sant'Angelo
Olummo
Tisichiello
Porticello
TM-23-3b
TM-23-20a
TM-21-2a
TM-20-5
TM-20-1c
TM-20-1b
TM-20
MgO (wt.%)
CaO (wt.%)
(a)
K_2O/Na_2O
CaO (wt.%)
(b)
Y (ppm)
Th (ppm)
(c)
Nd (ppm)
Th (ppm)
(d)

Fig 7

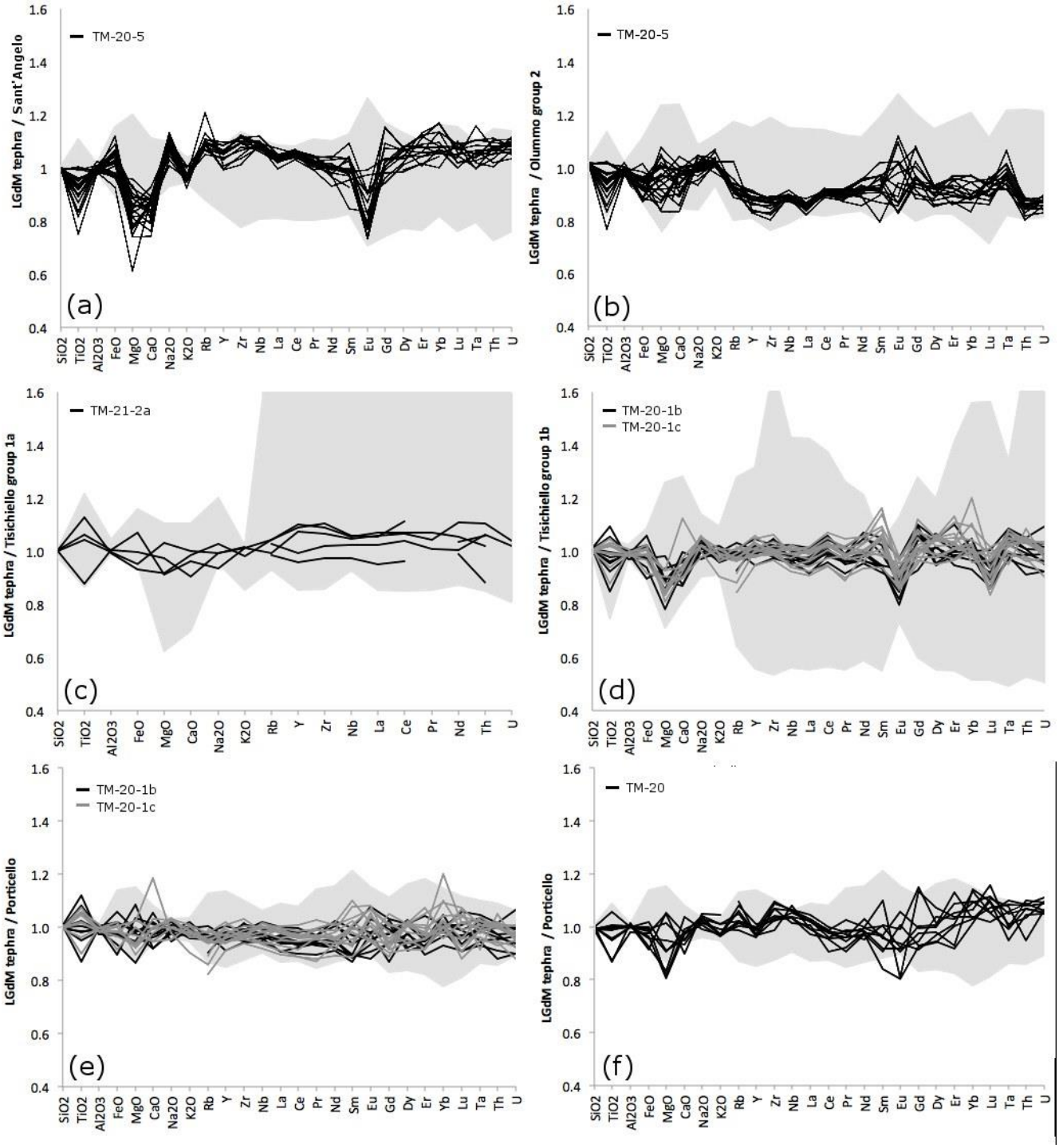
TM-20-5
LGdM tephra / Sant'Angelo
(a)
TM-20-5
LGdM tephra / Olummo group 2
(b)
TM-21-2a
LGdM tephra / Tisichiello group 1a
(c)
TM-20-1b
TM-20-1c
LGdM tephra / Tisichiello group 1b
(d)
TM-20-1b
TM-20-1c
LGdM tephra / Porticello
(e)
TM-20
LGdM tephra / Porticello
(f)
SiO2 TiO2 Al2O3 FeO MgO CaO Na2O K2O Rb Y Zr Nb La Ce Pr Nd Sm Eu Gd Dy Er Yb Lu Ta Th U

Fig 8

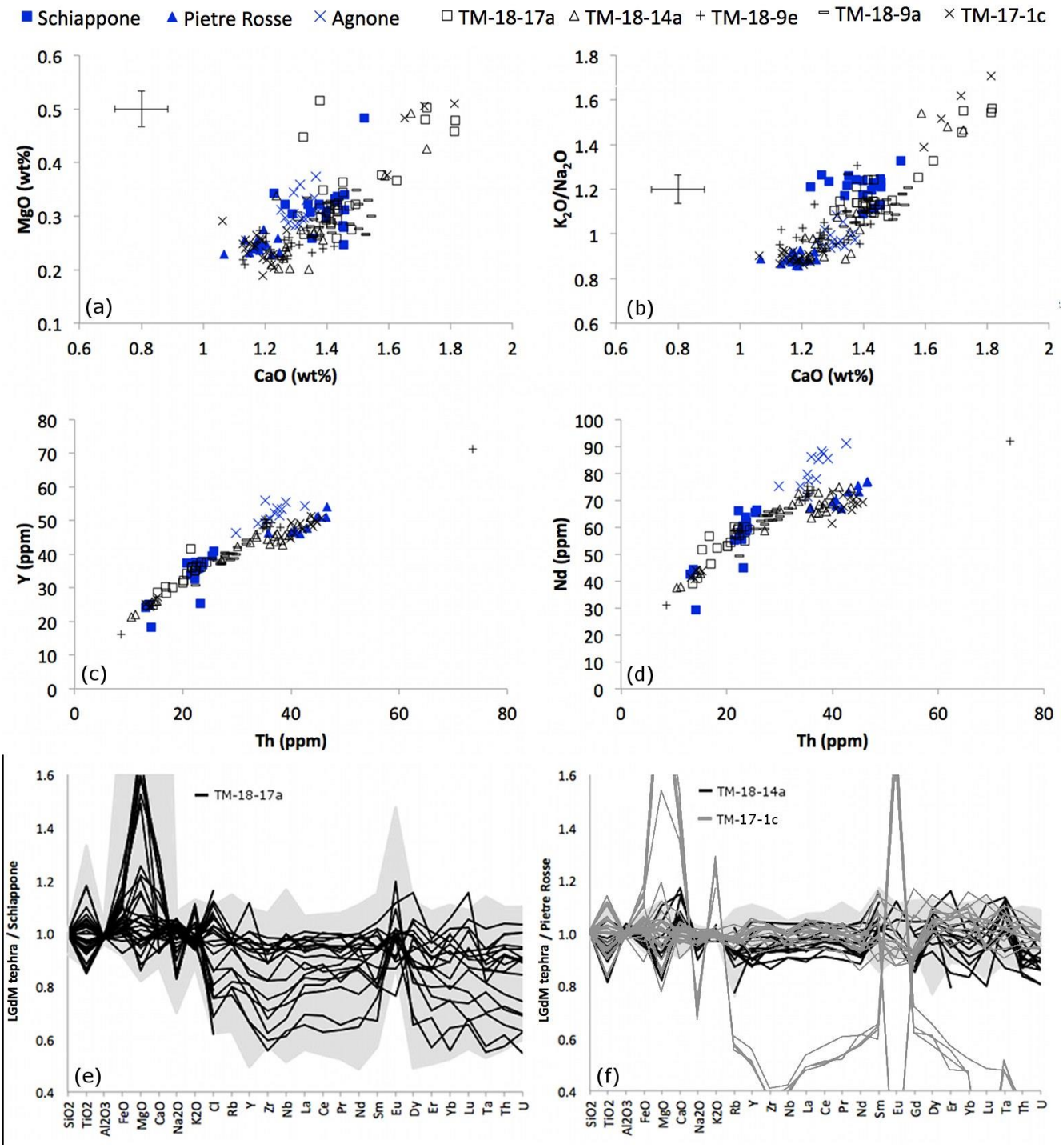
Schiappone
Pietre Rosse
Agnone
TM-18-17a
TM-18-14a
TM-18-9e
TM-18-9a
TM-17-1c
MgO (wt%)
CaO (wt%)
(a)
K_2O/Na_2O
CaO (wt%)
(b)
Y (ppm)
Th (ppm)
(c)
Nd (ppm)
Th (ppm)
(d)
LGdM tephra / Schiappone
TM-18-17a
(e)
SiO2 TiO2 Al2O3 FeO MgO CaO Na2O K2O Cl Rb Y Zr Nb La Ce Pr Nd Sm Eu Dy Er Yb Lu Ta Th U
LGdM tephra / Pietre Rosse
TM-18-14a
TM-17-1c
(f)
SiO2 TiO2 Al2O3 FeO MgO CaO Na2O K2O Rb Y Zr Nb La Ce Pr Nd Sm Eu Gd Dy Er Yb Lu Ta Th U

Fig. 9

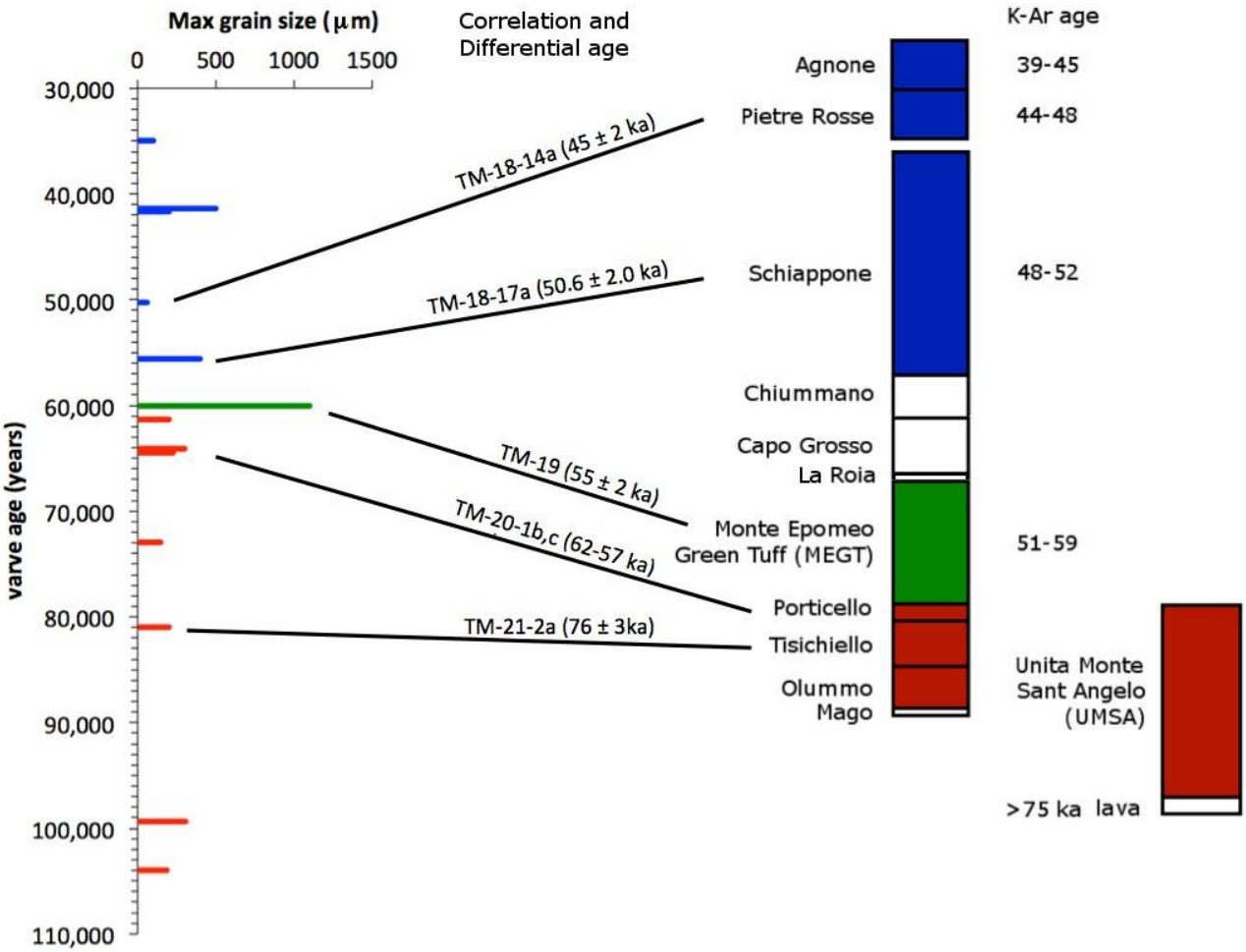
Max grain size (μm)
0
500
1000
1500
Correlation and
Differential age
K-Ar age
varve age (years)
30,000
40,000
50,000
60,000
70,000
80,000
90,000
100,000
110,000
TM-18-14a (45 ± 2 ka)
TM-18-17a (50.6 ± 2.0 ka)
TM-19 (55 ± 2 ka)
TM-20-1b,c (62-57 ka)
TM-21-2a (76 ± 3ka)
Agnone
Pietre Rosse
Schiappone
Chiummano
Capo Grosso
La Roia
Monte Epomeo
Green Tuff (MEGT)
Porticello
Tisichiello
Olummo
Mago
39-45
44-48
48-52
51-59
Unita Monte
Sant Angelo
(UMSA)
>75 ka lava

Fig 10